Journal of Geotechnical and Geo Computational Engineering

May - Aug 2025 Vol – 13 Issue – 2

ENRICHED PUBLICATIONS PVT. LTD

S-9, IIndFLOOR, MLU POCKET,
MANISH ABHINAV PLAZA-II, ABOVE FEDERAL BANK,
PLOT NO-5, SECTOR-5, DWARKA, NEW DELHI, INDIA-110075,
PHONE: - + (91)-(11)-47026006

Journal of Geotechnical and Geo Computational Engineering

Aims and Scope

The Journal of Geotechnical and Geo Computational Engineering aims at opening an easy access to the valuable source of information and providing an excellent publication channel for the global community of researchers /scholars/phd guides and phd pursuing students and others in the civil engineering subjects and especially geotechnology and its applications.

Typical subjects covered by this journal include:

- Computational and Theoretical Geomechnics
- Foundations
- Tunneling
- Earth Structures
- Site Characterization
- Soil-Structure Interactions

Journal of Geotechnical and Geo Computational Engineering

Managing Editor
Mr. Amit Prasad

Editorial Assistant
Mrs. Vandna Sharma

Editorial Board Member

Mohd. Masroor Alam
Asso. Prof. Engineering Geology
Dept. of Civil Engineering
Aligarh Muslim University

Dr. Pabitra Rajbongshi
Asso. Prof. Civil Engineering
Dept. NIT Silchar
E-mail: prajbongshi@yahoo.com

Journal of Geotechnical and Geo Computational Engineering

(Volume-13, Issue-2, 2025)

Contents

May - Aug 2025 | Vol – 13 | Issue - 2

A LABORATORY STUDY ON REPLACEMENT OF CONVENTIONAL PILES BY MICROPILES

Ashim Kanti Dey and **Dinesh Jamatia**
Professor Ex PG student
Civil Engineering Department
National Institute of Technology Silchar
Silchar, Assam – 788010

Abstract :

Soft clayey soil is abundantly available in many parts of India like Tripura, Assam, West Bengal, Bihar, Orissa, Uttar Pradesh, etc. The main problem with the soft clay is that this soil is highly susceptible to large settlement and possesses a very low bearing capacity. As such soft clay is not an accepted construction material. The best way to use this material is to construct piles for transferring the load to the hard strata below or to improve the ground. In case, the soft stratum is very thick the length of the piles becomes very large involving a high cost. Any ground improvement technique applicable to the soft clay is time consuming. Hence soft clay is described as a problematic soil to civil engineers. In the present study an attempt has been made to explore the possibility of use of micropiles to transfer the superimposed load to the soft soil itself. This will reduce the cost and time of construction. It is observed that a group of 4 conventional piles can effectively be replaced by 13 number of micropiles with the same loaded area and for equal settlement. Some parameters, such as loaded area of the pile group, number of piles in a group, area ratio and consistency of the soil have been found to be the major factors affecting the load carrying capacity of micropiles.

Introduction

Micropile is a small diameter (typically less than 300 mm), cast in situ replacement pile, which is built in a drilled bore hole with reinforcement and grout. The principle is initialized in Italy (Lizzi, 1978) in the 1950s to meet the necessity of retrofitting the old historical building and monuments. Micropiles can withstand axial and/or lateral loads, and may be considered a substitute for conventional piles or as one component in a composite soil/pile mass, depending upon the design concept employed as suggested by FHWA (2006).Reticulated micropiles were used for land stabilisation, reinforcement of quay walls, protection of buried structures, ground application techniques, etc. Research by Pearlman et. al. (1992) and Palmerton (1984) suggest that group of inclined micropiles serve to stabilise the sliding mass and thus can be used in slope protection work. Fondedile introduced the use of micropiles in North America in 1973 through a number of underpinning applications (FHWA, 2005). Use of micropiles did not grow rapidly in United States till 1980s when successful applications of micropiles were published. A proper use of micropiles can eliminate the demerits of conventional piles like negative drag force, large length, huge diameter and large project cost. Micropiles have also been used for improvement of bearing capacity of an existing footing. A ten-storeyed building, originally in a precarious condition due to differential settlement, was restored to safety using micropiles (Sridharan and Murthy, 1993). Perforated micropiles were used for retrofitting the foundations under dynamic loads (Shafigh and Seyrafian, 2011). 100 mm diameter and 4 m long micropiles were used to improve the bearing capacity of foundation soil and in the rehabilitation of the total building foundation system (Shivakumar Babu, et. al., 2004). Researchers (Tsukada, et. al.,1999) conducted a series of model tests on load carrying capacity of footings reinforced with micropiles installed in sand. They can be installed in access-restrictive environments and in all soil types and ground conditions. Design concept of micropiles is described in the report of Federal Highway Administration (FHWA, 2000). However, replacement of conventional piles by micropiles in soft clayey soil is a new proposition in India. Very little (almost no) work has been done on the subject area in India, In the present study model tests are carried out in soft clayey soil to study the load settlement behaviour of conventional piles vis-à-vis behaviour of micropiles having the same loaded area. Effects of various parameters, such as loaded area, number of micropiles, area ratio and consistency of the soil are studied.

Details of Model TestsA total of 10 number of model tests are conducted as per the details shown in Table. 1. The model tests are conducted in a rectangular steel tank of size 1500 mm x 600 mm x 900 mm height. The tank is filled with soft clayey soil of 700 mm depth. The clay lumps are dried, grinded, mixed with a required quantity of water and is allowed to undergo consolidation under its own weight for about 30 days. Out of ten tests five are conducted at water content more than the liquid limit of the soil and the remaining five are conducted at water content between the plastic and liquid limits of the soil. Two model tests are conducted with conventional piles, each of diameter 20 mm and the remaining tests are conducted with micropiles, each of diameter 6 mm. The length of both types of piles is kept as 150 mm. The thickness of pile cap is maintained as 20 mm and the cap is placed 20 mm above the soil surface so that the effect of pile cap on load transfer is eliminated. Detailed layout of the piles is shown in Fig. 1 and Fig. 2.

The soil in which model tests are conducted has the properties listed in Table. 2. The properties of the soil are found out by conducting Unconsolidated Undrained Triaxial test (UU) with pore water pressure measurement. The gradation curve of the soil is shown in Fig. 3 and is obtained by conducting wet sieve analysis and hydrometer analysis. The properties of micropiles are also shown in the table.

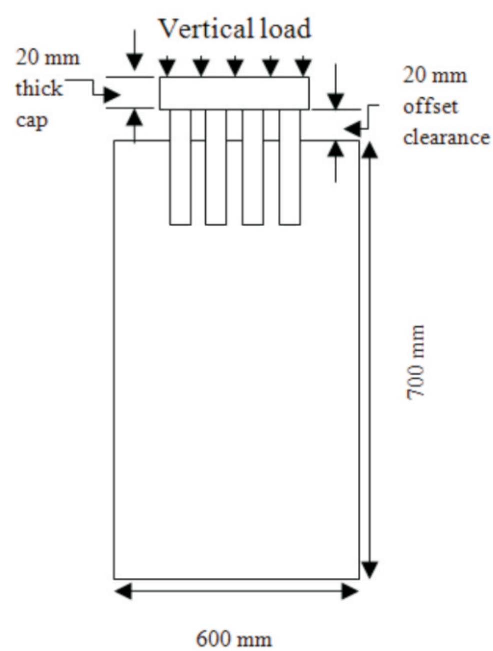

Fig. 1 Soil block loaded with 16 Micropiles.

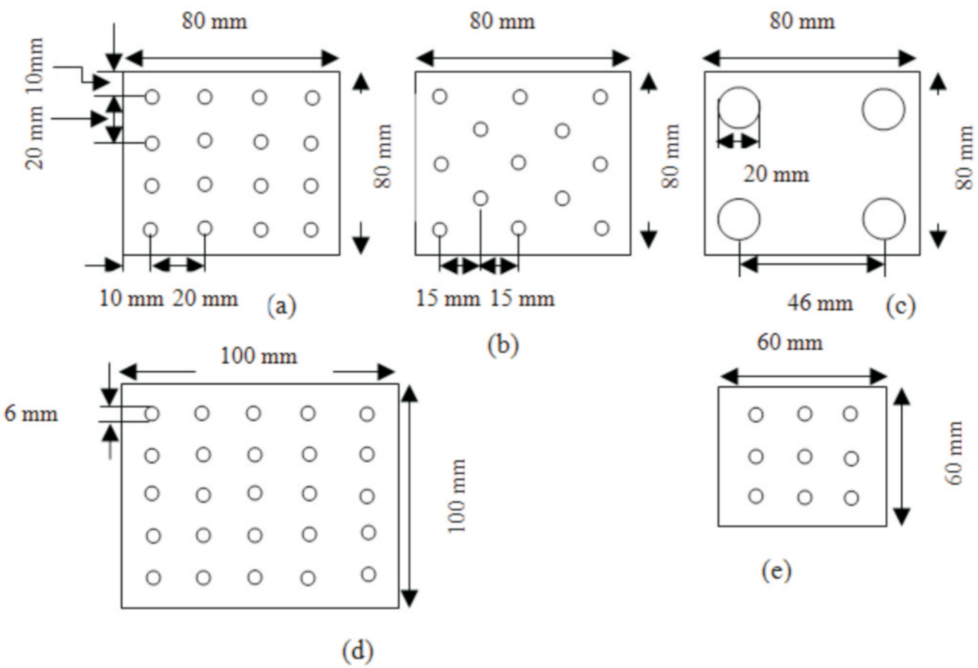

Fig. 2 Pile group arrangements (a) 16 micropiles (b) 13 micropiles (c) 4 conventional piles (d) 25 micropiles and (e) 9 micropiles.

Test no.*	Dia. of pile, d (mm)	Nos. of piles,	Loaded area, A** (mm^2)
1	6	16	66×66
2	6	13	66×66
3	20	4	66×66
4	6	25	86×86
5	6	9	46×46

** A = out to out dimension of piles
*Each test is conducted twice, one with water content more than liquid limit and the other with water content in between liquid limit and plastic limit

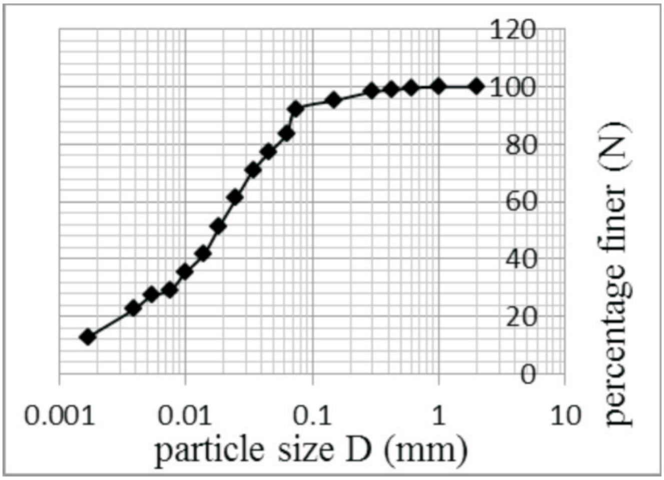

Fig 3 Particle size distribution of the soil.

Table 2 Properties of the materials used.

Soils		
Cohesion	22 kPa	
Angle of internal friction	0°	
Modulus of elasticity, E_s	630 kPa	
Poisson's ratio	0.4	
Piles		
	Micropiles (MP)	Conventional piles (CP)
Modulus of elasticity (Emp and Ecp)	14.1GPa	13.5 GPa
Bending stiffness (EI)	0.897 N-m²	106.02 N-m²

The modulus of elasticity of the soil is calculated as the slope of the stress-strain curve upto 1/2 to1/3 of the peak stress obtained from the UU test. The Poisson's ratio is taken from the literature available (Arora, 2009).

The model micropiles are made up of neat cement paste with centrally placed string rod of 1.5 mm diameter. The neat cement paste is prepared by using water-cement ratio of 0.5 as suggested by FHWA (2000) on account of pumpability and groutability. Whereas, the model conventional piles are made up of 1 (cement) : 2 (sand) with water/cement ratio of 0.65.

Similitude Ratio

Similitude ratio is the ratio of any linear dimension of the model to the corresponding dimension of the prototype (Shahu and Reddy, 2011). To reduce the total test duration, a minimum possible similitude ratio is desirable because of low permeability of the soil. A typical prototype micropile diameter varies from 0.1 to 0.3 m and length from 4-30 m. In the present model test, micropile of 6 mm diameter and 150 mm length is used which gives rise to a similitude ratio between 0.02 and 0.06. Generally, length to diameter (l/d) ratio in the prototype micropile varies between 13 and 100, based on which the l/d ratio in the model is adopted as 25. Typically a prototype conventional pile diameter varies from 0.3 to 6 m. In this study, model conventional pile of 20 mm diameter is used which gives rise to a similitude ratio between 0.003 and 0.067 with l/d ratio of 7.5.(length of pile being 150 mm).

Test Procedure

The micropiles are installed by a replacement method. A bore hole is made with an auger of diameter 6mm for micropiles and 20 mm for conventional piles. Cement slurry is injected into the hole followed by insertion of a 1.5 mm string rod at the centre. Three days after installation of micropiles, top soil layer of depth 25 mm is scooped out for the provision of 20 mm clearance between the micropile cap and the soil surface, the piles are inserted into the cap for a depth of 5 mm. The cap is constructed with proper shuttering and formwork. One week after the installation of the micropiles, the load tests are started in which the loads are applied on the micropile cap by placing dead weights. Equal loading increments are applied on the micropile cap and the corresponding settlements are recorded with the help of two dial gauges provided at opposite corners. Next load increment is given when the settlement of the pile group is less than 0.01 mm/hour. The model conventional piles are constructed by drilling a hole of 20 mm diameter with the help of an auger into the soil. A casing of 20 mm diameter is inserted and then the cement mortar is poured into the hole. Casings are particularly required when the water content of the soil is more than the liquid limit. As the cement mortar reaches approximately 1/3rd height of the hole, reinforcement cage is inserted into the bore hole. The casing is gradually withdrawn as the pouring of cement mortar continues; the up down movement of the casing imparts compaction of the cement mortar. Construction of pile cap and the loading sequence are similar to those applied for model micropiles.

Model Test Results And Discussions

Vertical loads on the micropiles are applied uniformly by placing specific weights (i.e. 2 kg, 4 kg, etc.) on the top of the pile cap. The load settlement curves are obtained. Other major parameters which influence the load settlement curve like influence area (A) of the group, modulus of elasticity of the soil (E_s), modulus of elasticity of the piles (E_{mp} and E_{cp}), area ratio (A_r), number of micropiles (N) have been studied discussed below.

Load-settlement behaviour of model micropile and conventional pile group

The settlements of different model micropile groups and conventional pile groups are observed under vertical loads. One set of test is done with water content above the liquid limit and the other set at water content within the plasticity index. Results are compared between pile groups having same loaded area and between pile groups of different loaded area. The load settlement curves are shown in Fig. 4 and Fig. 5. It is observed that for the same loaded area 16 micropile group takes more load than either 13 micropile group or 4 conventional pile group. Fig. 4(b) and Fig. 5(b) explain that more the loaded area more is the bearing capacity of the group irrespective of the consistency of the soil.

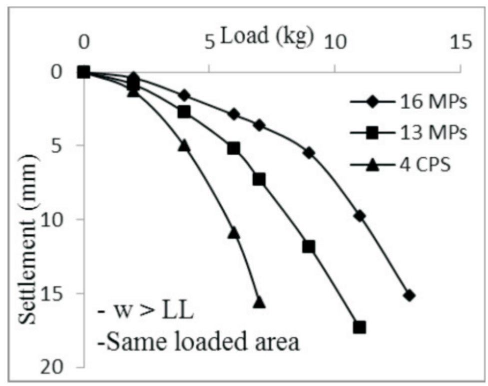

(a)

MP : micropile
CP : conventional pile

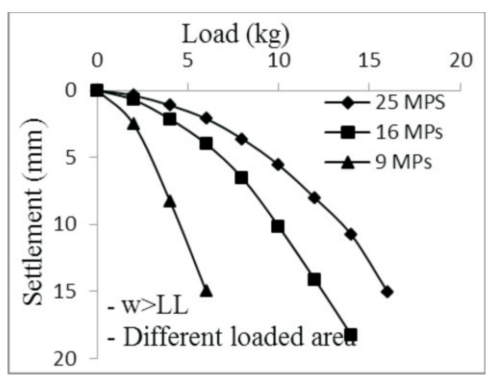

(b)

Fig.4 Load vs. settlement curve (a) same loaded area (b) different loaded area

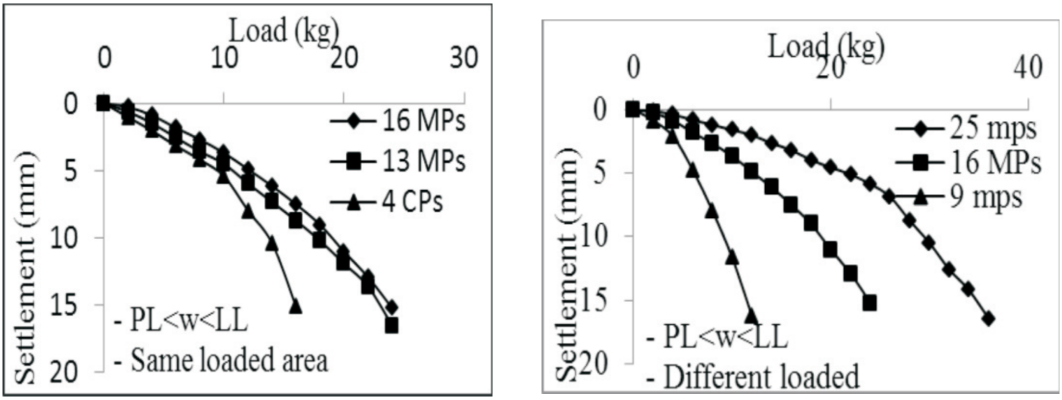

(a) (b)

Fig. 5 Load vs. settlement curve (a) same loaded area (b) different loaded area.

Table 3 shows the ultimate bearing capacity of the pile groups obtained by double tangent method (Venkatramaiah, 2006). From the table it is clear that 4 conventional pile group can effectively be replaced by 16 micropiles or 13 micropiles group.

Table 4 shows the quantity of materials required for the construction of the pile groups. It is observed that except steel reinforcement, consumption of materials is far less in micropile construction. This shows an encouraging result for replacement of conventional piles by micropiles.

Table 3 Ultimate load carrying capacity of the pile groups (Q_u).

Pile group	Ultimate load carrying capacity, Q_u (kg)	
	At w>L.L	At P.L<w<L.L
16 Micropiles	8.2	14
13 Micropiles	5.8	13
25 Micropiles	16	24.5
9 Micropiles	4.5	6.8
4 Conventional piles	4.6	11.5

Table 4 Quantity of materials required.

Pile group	Cement & Sand (mm^3)	String rod (mm^3)
16 Micropiles	63618	4240
13 Micropiles	51689	3445
25 Micropiles	99404	6625
9 Micropiles	35785	2385
4 Conventional piles	61772	3180

Effect of loaded area in load carrying capacity

Figure 6 shows the variation of load carrying capacity against the loaded area at any settlement. As expected, the load carrying capacity increases with increase in loaded area. The load carrying capacity of the conventional pile group is also shown in the figure. It is further concluded that for the same loaded area, the load carrying capacity of micropiles is more than that of conventional pile group. The load carrying capacity of the micropile group increases almost linearly with increase in loaded area.

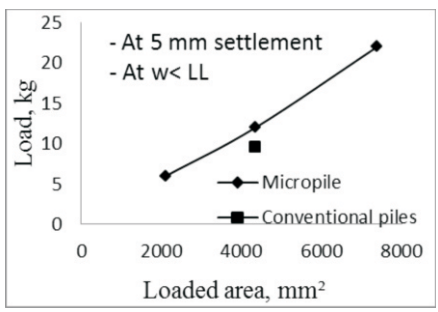

(a)

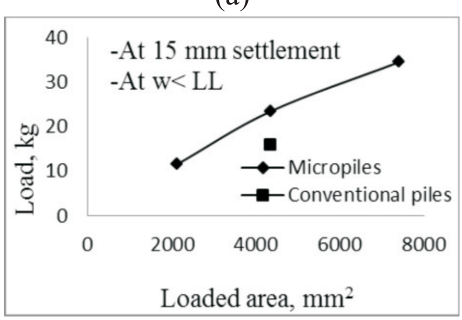

(b)

Fig. 6 Variation of load carrying capacity and loaded area (a) at 5 mm settlement (b) at 15 mm settlement .

Effect of area ratio in load carrying capacity

Area ratio (A_r) is defined as the ratio of the total cross-sectional area of the piles within the loaded area to the total loaded area of the pile group.

$$A_r = \frac{\text{Total cross sectional area of the pile}}{\text{Total loaded area}}$$

Fig. 7 shows that the load carrying capacity of the pile group increases with the increase in its area ratio till it reaches the optimum value and then decreases with further increase in the area ratio. This tendency is applicable at any given settlement.

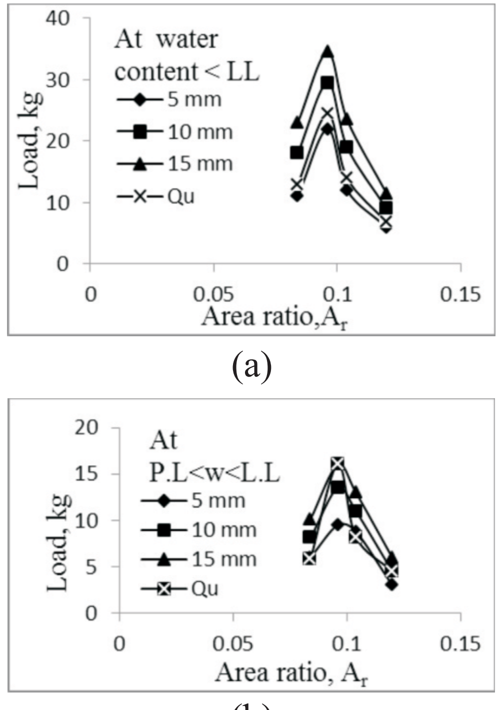

Fig. 7 Variation of load carrying capacity against area ratio (a) at water content, w >LL, (b) PL<w<LL.

Improvement Factor

A term called Improvement factor (I.F) can be defined from the present study as the ratio of the load taken up by the micropile group to the load taken up by the conventional pile group with the same loaded area for a specified amount of settlement. Thus the improvement factor can be directly correlated with the improvement in the bearing capacity of the micropile group. Thus for a given loaded area and for a given settlement, the Improvement factor is defined as

$$I.F = \frac{\text{Load capacity of micropile group}}{\text{Load capacity of conventional pile group}}$$

Fig. 8 shows the variation of the improvement factor against settlement for 16 micropile group and 13 micropile group. It is observed that although the improvement factor is more than one, the improvement factor shows an increasing trend with the increase in settlement for water content less than the liquid limit and shows a decreasing trend for water content above the liquid limit

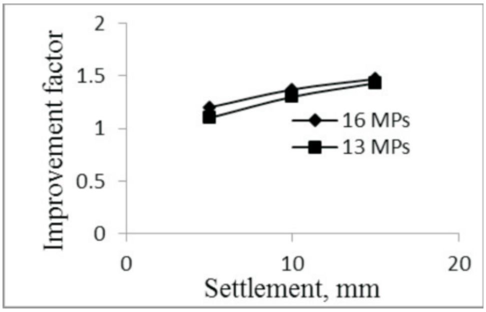

(a)

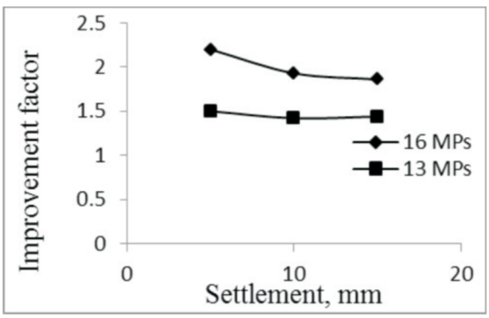

(b)

Fig. 8 Settlement vs. Improvement factor, (a) at P.L<w<L.L, (b) at w>L.L.

Conclusions

Following conclusions are drawn from the present study:

1. The major parameters that influence the settlement behaviour of the micropile groups are applied vertical stress on the top of the micropile cap (Q), loaded area (A) of the group, modulus of elasticity of soil (E_s), number of micropiles (N) and area ratio (A_r).
2. The more the number of piles in a group more is the load carrying capacity irrespective of their arrangements and consistency of the soil.
3. Four conventional piles group can effectively be replaced by using 16 micropiles or 13 micropiles group from the ultimate bearing capacity point of view irrespective of the consistency of the soil. It is also found that the conventional piles can be economically replaced by 16 micropile group or 13 micropile group.
4. Instead of using bulky, large diametered inconvenient conventional piles, few number of small diameter piles (i.e., micropiles) can be effectively used to support a given vertical load.

References

1. Arora K.R. (2009), *Soil mechanics and foundation engineering*, reprint edition, Standard Publishers Distributors, Delhi
2. Lizzi, F. (1978), "Reticulated root piles to correct Land slides", *Proc. of ASCE Conference*, Chicago, Illinois, October, 16-20.
3. Masoud Alizadeh Shafigh, and Sarang Seyrafian (2011), **Perforated Micropiles Systems for Retrofitting of Foundations under the Dynamic Loads,** *International Journal of Earth Sciences and Engineering* ISSN 0974-5904, Volume 04, No 06 SPL, October 2011, pp 15-18.
4. Micropile Design and Construction Guidelines Implementation Manual, FHWA-SA-97-070, June, 2000.
5. Shahu J. T. and Reddy Y. R. (2011), Clayey Soil Reinforced with

Stone Column Group: Model Tests and Analyses, *Journal of geotechnical and geoenvironmental engineering*, Dec. 2011.

6. **Sivakumar Babu G.L., Srinivasa Murthy B. R., Murthy D.S. N. and Nataraj M.S.** (2004), *Bearing capacity improvement using micropiles a case study, Geosupport 2004, geosupport conference:Innovation and cooperation in the geo-industry*, 29-31, January, 2004, Orlando, Florida, pp. 1-8.

7. Sridharan, A., and Murthy, B.R.S. (1993), Remedial measures to building settlement problem, *Proceedings of Third International conference on case histories in Geotechnical Engineering*, St. Louis, Missouri, 221-224.

8. Tsukada Y., Miura k., Tsubokawa Y., Otani Y., You G. L. and Ishito M., Nishimura (1999), Experimental investigation on the imicropilerovement of bearing capacity of surface footing with micropiles, *Proceedings on the 2nd international workshop on Micropiles*, September, Ube city, Japan: 139 – 148.

9. Venkatramaiah C. (2006), *Geotechnical Engineering*, revised third edition, New Age, New Delhi.

ESTIMATION AND QUANTIFICATION OF URBAN FLOOD VULNERABILITY AT WARD LEVEL USING GEOSPATIAL TECHNOLOGIES – A CASE STUDY OF DEHRADUN, INDIA.

V.V. Saikrishna[1], **Kamal Pandey** [2]

[1]Indian Institute of Technology Bombay, Mumbai, India, 400076.
[2]Indian Institute of Remote Sensing, Dehradun, India, 248001.
Email: vsaikrishna1990@gmail.com, kamal@iirs.gov.in
Mobile No.: +91 9004318488, +91 9634629886

Abstract

Drastic variation in urban micro-climate pattern in recent years advances the occurrence of high intensity rainfall and as a result flood like situation has been observed in urban areas. The urban floods results in both direct and indirect losses to the people, infrastructure, animals, industries and other assets of the city. Remote sensing and GIS plays a prominent role especially in urban flood vulnerability analysis, risk assessment, risk management issues, hazard mapping and damage assessment issues, etc. Dehradun is a capital city and getting urbanized at a gigantic growth rate, in this process the existing inhabited areaas well as pervious surfaces are becoming impervious surfaces and disallowing the excess rainfall to percolate into the soil. Also the present city's drainage network is very old and in a rundown condition which results in water logging during high rainfall events. In the present research, an attempt is made to estimate the urban flood vulnerability index and quantify it at a ward level for Dehradun city using geospatial techniques. Geospatial data set from multiple sources with unique characteristics have been used in the study, which includes elevation data and satellite images of multi date and resolution. Multi criteria decision making technique was used for calculating the urban flood vulnerability index. Based on the vulnerability index the municipal wards of the city are classified as high, medium and low vulnerability zones.

Keywords: *Urban flood, Multi criteria analysis,* vulnerability index

1. Introduction

Floods in the urban area primarily results due to improper planning of the drainage system.The changes in land use land cover (LULC) increases impervious ground surfaces consequently decreasing infiltration rate and increasing runoff rate. The driving factors of urban flood risk includes increase in vulnerability associated with population growth, economic development, urbanization, poverty . Also there is a significant difference in urban flooding as compared to rural flooding.

Remote sensing (RS) and GIS plays a prominent role especially in urban flood vulnerability analysis, risk assessment, risk management issues, hazard mapping and damage assessment issues, etc. Another advantage of RS images is its temporal nature and spatial variability which can be exploited for successful hydrological analysis, prediction and validation. RS images can be used to detect the changes in the land use caused due to either natural or human activities. Hydrological modelling is extensively practiced in the planning and development of integrated approach for the management of water resources by the research hydrologist and practicing water resources engineers. concluded that the runoff response to rainfall inputs can be accurately determined for describing watershed characteristics with available spatial data and existing computational power. Geographic information system (GIS) and remote sensing techniques facilitates hydrological modelling process and makes hydrological catchments models near to physical process .

One of the studies carried out by focused on flooding events of four rapidly expanding mega cities of India viz. Delhi, Kolkata, Mumbai and Chennai. The study used daily rainfall data two station in each city (1970-2006) apart from it the data from disastrous weather events published by India Meteorological Department have also been used. studied the Chennai Metropolitan Areas for urban flooding impacts, they observed that in spite of negative trend in average rainfall over the period of last 20 years, there is a contrast record of increasing floods in Chennai. carried out a case study in Noida city to quantify the factors causing of urban flooding. They observed that rapid urbanization has resulted in losses of farmland, forest and shrub since 1995 as more than 36% of the forest and 22% of the shrub areas were transformed into farmlands and settlements. Another study carried out for the city of Gorakhpur in Indiaby performed spatial risk analysis using past sample flood events using MODIS data. The study was carried out to quantify spatial extent of flood-affected areas for the years 1998 and 2007.

Dehradun is a capital city and getting urbanized at a gigantic growth rate, in this process the existing inhabited area as well as pervious surfaces are becoming impervious surfaces and disallowing the excess rainfall to percolate into the soil. Also the present city's drainage network is very old and in a rundown condition which results in water logging during high rainfall events. In the present research, an attempt is made to estimate the urban flood vulnerability index and quantify it at a ward level for Dehradun city using geospatial techniques. Geospatial data set from multiple sources with unique characteristics have been used in the study, which includes elevation data and satellite images of multi resolution. Multi criteria decision making technique has been used for calculating the flood vulnerability index. Based on the vulnerability index the municipal wards of the city are classified as high, medium and low vulnerability zones.

2. Study area

Dehradun, the capital city of Uttarakhand is situated in south central part of Dehradun district, Uttarakhand, India and it is shown in figure 1. Dehradun is divided into 60 wards with an area of 64.88 sq. km which is located between 77°59'5" west, 78°6' 4"east longitudes and 30°16'10” south, 30°24' 19" north latitude.

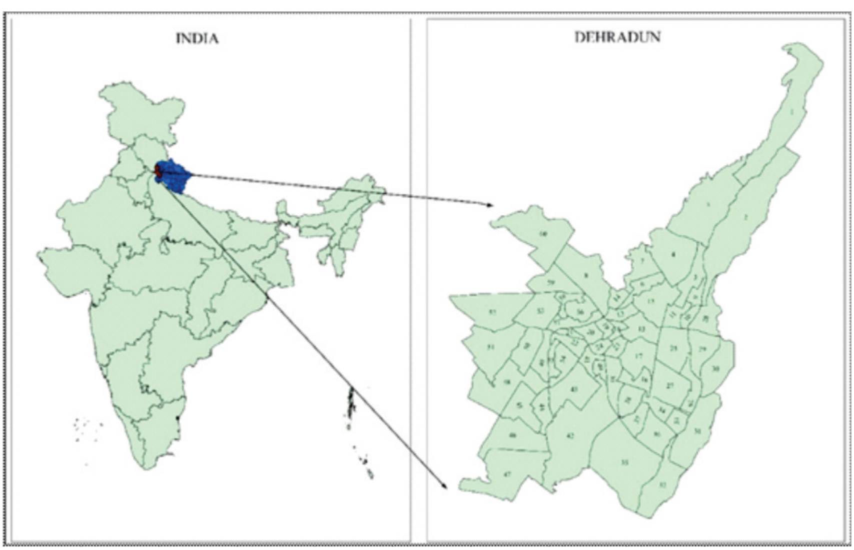

Figure 1: Study area map of Dehradun

3. Data used

To analyze the hydrologic process of watersheds in Dehradun both primary and secondary data was used. The secondary includes data collected from various organizations like Climate Forecast System Reanalysis (CFSR), Dehradun nagar nigam, Census of India, NBSS&LUPand variousother government bodies. The primary data includes field visits and locating the water logged areas through GPS device. Remote sensing data used in the research is shown in table 1. Also ASTER DEM acquired from USGS was used for terrain modelling and hydrologic elements generations. ASTER DEM has a horizontal spatial resolution of 30 meters.

Table 1: Data sets used in the research

Satellite	Sensor	Date of acquisition	Spatial resolution
1. IRS-P6	LISS-IV	• 28th March 2010 • 7th March 2013	5.6 m
2. Landsat 8	OLI	• 17th April 2015	30 m

4. Methodology

The remote sensing data was preprocessed before subjecting it to analysis process. Arc Hydro Tools was used for pre-processing ASTER-DEM (The Advanced Space borne Thermal Emission and Reflection Radiometer – Digital elevation model) and a depression-less DEM was created. Entire geoprocessing tasks were carried out in raster format at a spatial resolution of 30 meters. Land use land cover map was generated by hybrid classification method from LISS-IV data and master plan of Dehradun city. Location of rain gage stations were interpolated to get the spatial distribution of rainfall, and to know which part of the study area is covered by which rain gauge station. Soil map was generated using maps obtained from National Bureau of Soil Survey and validated by overlaying it over geo-referenced IRS P6 LISS-IV satellite image. The soil map thus generated was reclassified into hydrological soil group map which is useful in hydrological analysis of watersheds. Dehradun is falling under only two hydrological soil groups “A” and “D”.

Rainfall curve number (CN) is defined as a coefficient that diminishes total precipitation into runoff potential, after losses, so higher CN value represents higher runoff potential and vice versa. A CN look up table was created with the columns A, B, C, D which store curve numbers for corresponding soil groups for each land use category. These curve numbers were obtained from SCS TR55(Cronshey, 1986). Land use land cover and Hydrological Soil Group map (HSG) were generated to calculate Curve Number and for the preparation of rainfall-runoff model by the mean of HEC-HMS.

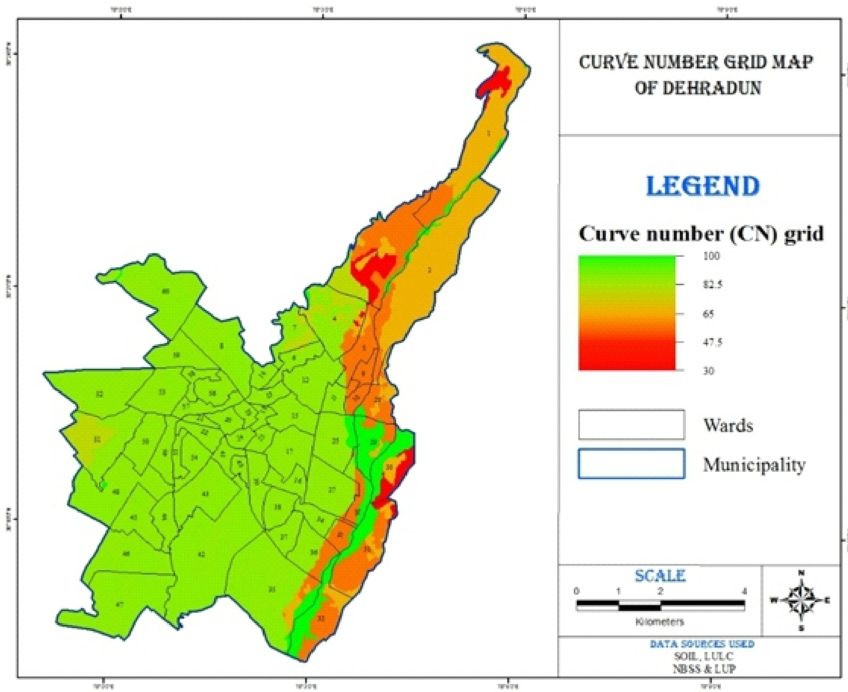

Figure 2: CN grid map of Dehradun

SCS Curve number grid was generated by combining LULC and soil map with CN look up table (Fan et al., 2013)which is used by many hydrologic models to extract the curve number for watershedsas shown in the figure 2. Stream network was generated from the processed DEM by defining a threshold of 0.15 for area field in square kilometers. The generated streams were segmented as either a head segment or a segment between two segment junctions. Watersheds were also delineated from the processed DEM by running a series of geo processing tasks such as flow accumulation, Flow direction, Stream definition, Stream Segmentation, Catchment Grid Delineation, Catchment Polygon, Drainage line, Adjoint Catchment processing and Drainage point processing. A geometric network was established to create a relationship between all the elements of a watershed with water flow direction.The watersheds of the study area are shown in the figure3.HEC-Geo HMS was used in creating HEC – HMS model for all the watersheds—(Martin et al., 2012). It is mainly helpful in creating the inputs required by HEC – HMS model such as average slope value, river length, basin area, curve number and CN lag time for rainfall runoff model. The HEC-HMS model of the water shed 1 is HEC-HMS model was designed to simulate the precipitation-runoff processes of watershed systems to identify drainage and overland flow and forecasting based on the resulted hydrograph. Dehradun is coming under five watersheds. These watersheds are again sub divided into sub – basins for detailed analysis of rainfall runoff simulations. There are four main components namely Basin model manager, Metrologic model manager, Control specification manager and Time – series data manager in HEC-HMS(U.S. Army Corps of Engineers (USACE), 1964) that were used to define characteristics of elements in a hydrologic network. Physically watershed was represented by a basin model where hydrologic elements (source, reach, sub-basin, junction, reservoir, diversion, and sink) are connected in a dendritic network to simulate rainfall runoff processes. Precipitation data was input through the time series data manager. Manually each sub basin must assign to a rainfall gage by its spatial coverage i.e. thiessen polygons and daily rainfall data from 01.01.1979 to 31.07.2014 was used for simulation. In control specification manager the time period was set from 01.01.2000 to 31.07.2014. To calculate peak discharge SCS Curve Number Loss method, SCS unit hydrograph transform method and CN lag time was used. After simulating the rainfall, runoff and peak discharge values are obtained for each sub basin. All five water sheds are to be modelled in the same manner to get peak discharge value of all sub basins in the study area.

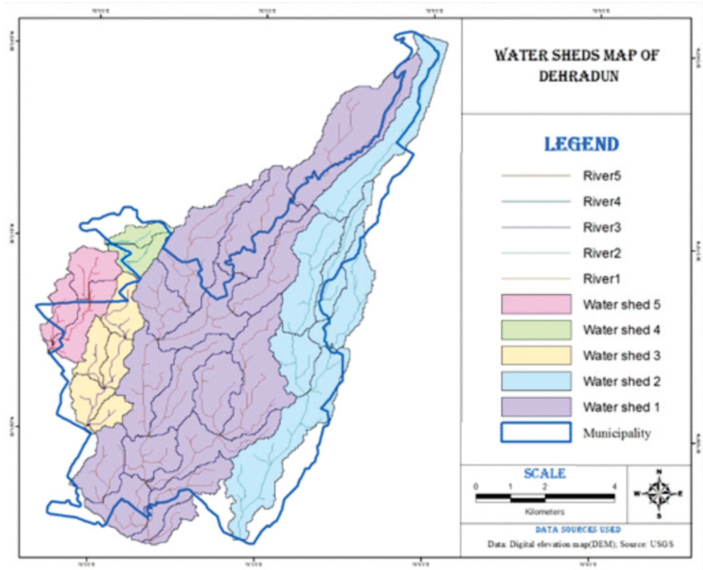

Figure 3: Water sheds map of Dehradun

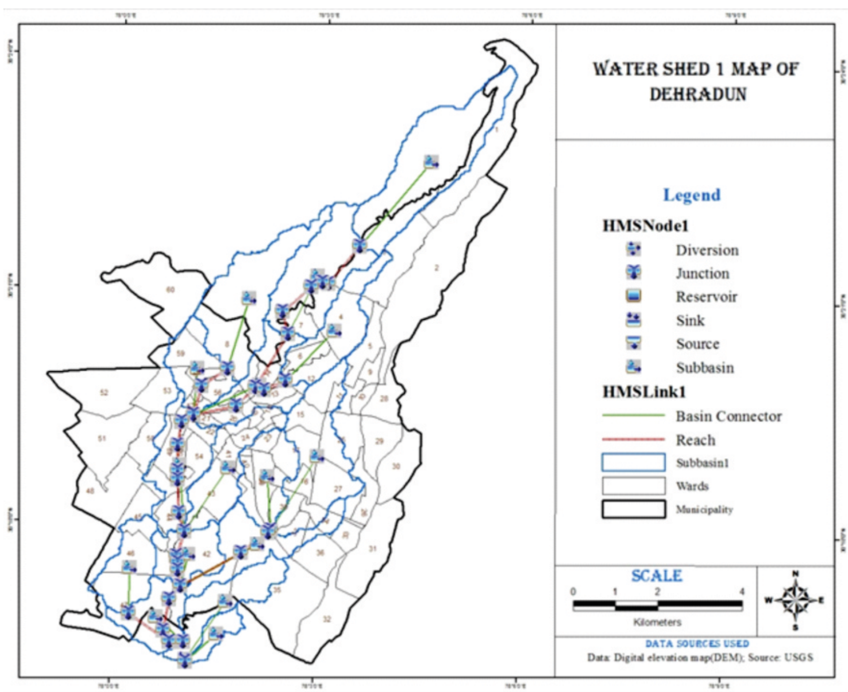

Figure 4: HEC-HMS model of the water shed 1

4.1 Weighted overlay analysis:

A total of six criterias namely peak discharge, hospitals, institutions, Normalized difference built up index (NDBI), population density and roads were considered in defining ward wise flood vulnerability map of Dehradun. All criterias were reclassified to a common scale for performing the weighted overlay analysis. The sub criterias of hospitals, institutions, roads were reclassified on 2 – 10 scale by manual classification, NDBI and population density were reclassified by natural jerks classification. The weightages are shown in table 2. Finally a ward wise flood vulnerability map was generated.

Table 2: Weightages given to the main criterias

Criterias	Weightages
1. Peak discharge	35
2. Hospitals	10
3. Institutions	10
4. NDBI	15
5. Population density	10
6. Roads	20

5. Results and conclusions

The peak rainfall discharge map obtained from the rainfall runoff simulation is shown in the figure 5. The results obtained from weighted overlay analysis shows that core area of the city is at higher risk and it is shown in the figure 6. The areas that are spatially located outwards of the city are at medium and low risk, the main reasons for this phenomenon is that urbanization process has geared uptremendously in last 10 years after Dehradun was declared as the capital city of newly formed Uttarakhand state.There aresome gaps in the resultant map which aredue to non-coverage of water sheds throughout the study area. This can be further improved by considering the water sheds at greater spatial extent so that the entire city is covered. Ward wise flood vulnerability map was obtained by taking different weights of number of pixels of three classes namely low, medium and high vulnerabilities.The results may deviate from the true scenario for the wards 2, 31, 46, 47, 48, 51, 60 because of gaps present in the final vulnerability map. For each ward a weightages of 3, 6, and 9 are multiplied with low, medium and high flood vulnerability classes and averaged it by dividing the sum of number of pixels of all the classes. The resultant map was reclassified into five classes such as very low, low, medium, high, very high to show the variability of flood vulnerability and it is shown in the figure 7.

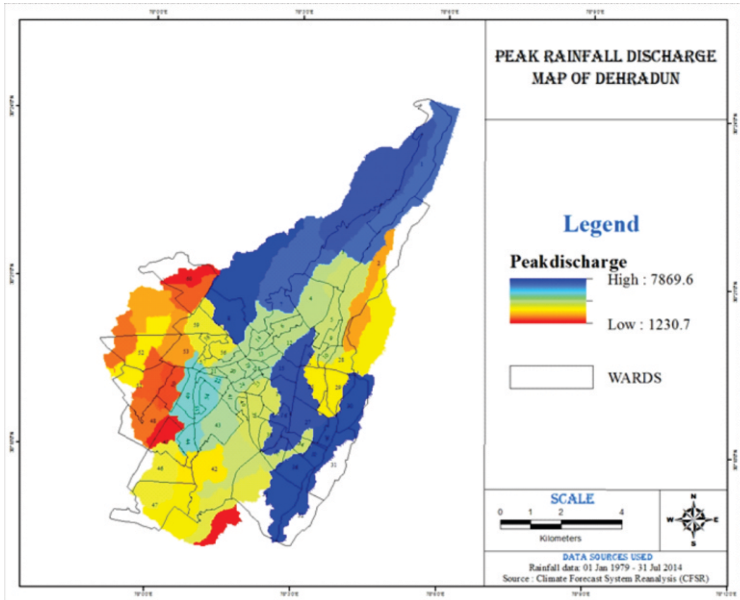

Figure 5: Peak rainfall discharge map of the study area.

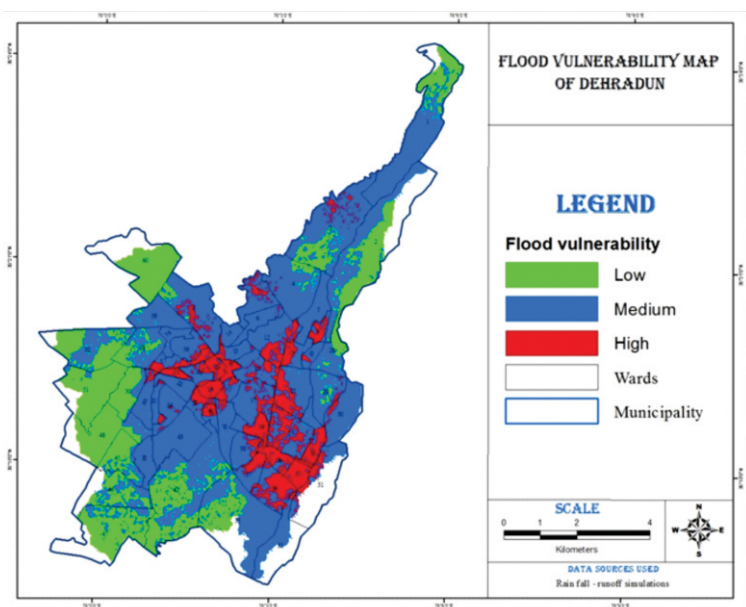

Figure 6: Flood vulnerability map of the study area

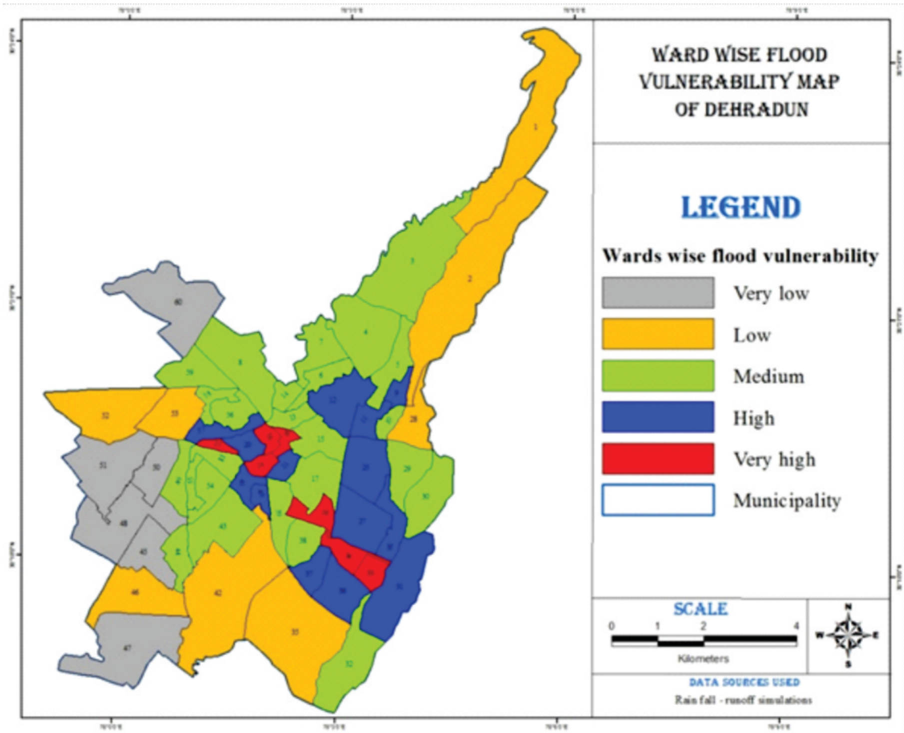

Figure 7: Ward wise flood vulnerability map

References

1. Abhas Jha, 2011. Urban Flood Risk Management for the 21st Century.

2. Arwa D. O., 2000. GIS Based Rainfall Runoff Model for the Turasha Sub Catchment Kenya. International institute for aerospace survey and earth sciences, Enschede, The Netherlands, Netherlands.

3. Cronshey, R., 1986. Urban hydrology for small watersheds. US Dept. of Agriculture, Soil Conservation Service, Engineering Division.

4. De, U.S., Singh, G.P., Rase, D.M., 2013. Urban flooding in recent decades in four mega cities of India. J Ind Geophys Union April 2013 17, 153–165.

5. Fan, F., Deng, Y., Hu, X., Weng, Q., 2013. Estimating Composite Curve Number Using an Improved SCS-CN Method with Remotely Sensed Variables in Guangzhou, China. Remote Sens. 5, 1425–1438. Doi: 10.3390/rs5031425

6. Gupta, A.K., Nair, S.S., 2011. Urban floods in Bangalore and Chennai: risk management challenges

and lessons for sustainable urban ecology. Curr. Sci. 100, 1638–1645.
7. Jagadeesha, C. J., 1999. Water Resources Development and Management, Asia's first GIS/GPS/RS/ monthly magazine.
8. Jain, S.K., Singh, R.D., Seth, S.M., 2000. Design Flood Estimation Using GIS Supported GIUHApproach. Water Resour. Manag. 14, 369–376. Doi: 10.1023/A:1011147623014
9. Martin, O., Rugumayo, A., Ovcharovichova, J., 2012. Application of HEC HMS/RAS and GIS tools in flood modeling: A case study for river Sironko – Uganda. 1(2), 19–31.
10. NDMA, GOI, 2010. National Disaster Management Guidelines: Management of Urban Flooding.
11. Singh, R.B., Singh, S., 2011. Rapid urbanization and induced flood risk in Noida, India. Asian Geogr. 28, 147–169. doi:10.1080/10225706.2011.629417
12. S. Mohan, Madhav Narayan Shrestha, 2000. A GIS based integrated model for assessment of hydrological changes due to land use modifications [WWW Document]. URL http://ces.iisc.ernet.in/energy/water/proceed/section5/paper1/section5paper1.htm (accessed 8.31.15).
13. Taubenböck, H., Wurm, M., Netzband, M., Zwenzner, H., Roth, A., Rahman, A., Dech, S., 2011. Flood risks in urbanized areas – multi-sensoral approaches using remotely sensed data for risk assessment. Nat. Hazards Earth Syst. Sci. 11, 431–444. Doi: 10.5194/nhess-11-431-2011
14. U.S. Army Corps of Engineers (USACE), 1964. HEC-GeoHMS [WWW Document]. US Army Corps Eng. USACE Hydrol. Eng. Cent. CEIWR-HEC. URL http://www.hec.usace.army.mil/software/hec-geohms/ (accessed 8.31.15).

Acknowledgements

Authors are thankful to Director of Indian Institute of Remote Sensing (IIRS) and Head of the department URSD, IIRS for their valuable guidance and suggestions.A very special thanks to B.D.Bharath,Dr. Stutee Gupta and all other faculty members in IIRS for helping and guiding at various junctures during the research.Authors are thankful to all officials in Uttarakhand Jal Sansthan and Mott MacDonald consultant for providing the data. Authors would also like to extend their deepest gratitude to Head C-USE, IIT Bombay and other faculty members of the department for their guidance and suggestions.

ICE THICKNESS ESTIMATION USING GEOSPATIAL TECHNOLOGY

Sanjay Manohar Bisht[1]
Praveen Kumar Thakur[1], **Arpit Chouksey**,[1]
Shiv Prasad Agarwal[1]

[1]Water Resources Department, Indian Institute of Remote Sensing,
4-Kalidas Road, Dehradun-248001, India
Email**:** praveen@iirs.gov.in

Abstract

The present study estimates ice thickness distribution over the Gangotri group of glaciers using modelling techniques. The modelling techniques follows the flow law of ice and empirical relation between the slope and height relation found for glacier system over the world. Surface velocity was calculated using multi-temporal PAN data from Landsat 7/8 (15m) and Indian Remote Sensing Satellite IRS-1C/1D (5m) data over the years 1998 to 2014. This study uses for the first time IRS-1C/1D for Gangotri glacier velocity estimation. Sub-pixel correlation of the images were done using COSI-Corr software. The study was able to successfully conclude the measured velocity to that of 0.02m/day for the duration of 1998-2014 over the whole glacier. Velocity over accumulation zone was found to be 0.041m/day. Also the modelled ice depth was analyzed and found to be in range of 58 to 450 m for the entire glacier. Few small area in middle and upper part of glacier showed values between 450-650m. The ice depth found at snout varied from 58 m to 67 m. Finally the modelled depth was correlated to the Terrestrial Laser Scanner (TLS) field measurements and was found to be in having a correlation of R^2=0.79. The estimated ice depth matches well with earlier reported studies for Gangotri glacier.

Keywords: Glacier Velocity, Landsat, IRS 1C/1D, Ice flow model, Glacier Depth, TLS, Glacier dynamics

1. Introduction

The Himalayan–Karakoram (HK) region has the largest glacier coverage outside the Polar Regions but knowledge of the dimensions of these glaciers and their behavior in response to climate change is still limited, due to their remoteness, the harsh topography, the complex political situation, and the associated difficult physical access (Bolch et al., 2012). Glaciers influence the runoff regime of major river systems affecting millions of people down river (Immerzeel et al., 2010; Kaser et al., 2010). Of these glaciers, the Gangotri group of glacier is a prominent system of glaciers as it is the first source of water in the Ganga Basin affecting large part of north India. Furthermore, applications of modern methodologies, such as measurements of gravity field anomalies (Jacob et al., 2012) or laser altimetry (Kääb et al., 2012), and combinations of them with field data (Gardner et al., 2013) lead to deviating findings, underlining the difficulty of measuring complex processes in such a large region.Two of the major parameters used to characterize glacier dynamics are surface velocity and ice thickness (Gantayat et al., 2014). In this work, therefore, we estimate the ice thickness distribution over Gangotri Glacier. The surface velocities were estimated using feature tracking based techniques using medium to high resolution ortho-rectified and co-registered remote-sensing data (Leprince et al., 2007). Here, we also focus on determining the ice depth for the Gangotri group of glacier, which is a basic parameter required for glacier melt projections (Huss et al., 2008; Gabbi et al., 2012), and estimates of future sea-level rise contributions due to glacier melt.

To estimate glacier volumes various methods have been proposed over time, such as volume–area (V–A) relations (e.g., Chen and Ohmura, 1990; Bahr et al., 1997), slope-dependent ice thickness estimations (Haeberli and Hoelzle, 1995), and more recently spatially distributed ice-thickness models (Linsbauer et al., 2009; Cuffey and Patterson, 2010; Huss and Farinotti, 2012; Li et al., 2012; Clarke et al. 2013). Power-law relationships for volume/area, volume/length and volume/area/length have been derived from the abundant information available regarding area and length (Chen and Ohmura, 1990; Bahr et al., 1997; Radić et al., 2010). First estimate of the ice thickness distribution of all glaciers around the globe was presented by Huss and Farinotti (2012). Artificial neural network methods have also been employed, using calculations based on a digital elevation model (DEM) and a mask of present-day ice cover in the Mount Waddington area in British Columbia and Yukon, Canada (Clarke and others, 2009). These networks are trained by substituting the known topography of ice-free regions, adjacent to the ice-covered regions of interest in case of non-availability of data providing maximum relative uncertainty in volume estimates at 45%. Ice volume was calculated for Columbia Glacier, Alaska, USA, by estimating ice fluxes using the equation of continuity between adjacent flowlines (McNabb and others, 2012).

In that investigation surface velocities and mass balance were used to estimate mean ice flux. Farinotti and others (2009a) developed another approach, using apparent mass balance to estimate ice thickness. From a distribution of apparent mass balance, ice flux was computed over selected ice flowlines and was then converted to ice thickness using Glen's flow law (Glen, 1955). Using this method, the ice-thickness distribution and volumes were estimated for glaciers in the Swiss Alps and elsewhere (Farinotti and others, 2009b; Huss and Farinotti, 2012). Mass-balance distribution data over large glaciers in the Himalaya are not easily available and are inaccurate in some cases (Bolch et. al.,2012).

Here, we present ice volume estimations for the Gangotri group of glacier using three different V–A relations, a slope-dependent ice thickness estimation method, an ice-thickness distribution model and a model using surface velocities, slope and the flow law of ice. These methods are applied to the same base data, comprising the 90 m digital elevation model (DEM) from the Shuttle Radar Topography Mission (SRTM). Results from the different approaches are then correlated at snout using the Terrestrial laser Scanner (TLS) based ground survey during 15-17 Sep. 2014.

1.1 *Study region and data*

The study area consists of the Gangotri group of glacier in the Gharwal Himalayas of India. The Gangotri glacier is one of the largest glaciers in the Himalayas, being approximately 30 km long with a width varying between 0.5 and 2.5 km. It has a height varying between 4000 and 7000 m.a.s.l. (Jain, S.K., 2008). The Gangotri glacier is a valley type glacier, flowing into the NW direction. Of the Gangotri glacier, approximately 29% of the total area is affected by debris. The three main tributaries are Raktvarn (15.90 km), Chaturangi (22.45 km) and Kirti (11.05 km) (Figure 1) and five other tributaries contribute to the Gangotri glacier. The present land forms are the result of erosion and deposition processes of glacial-periglacial features.

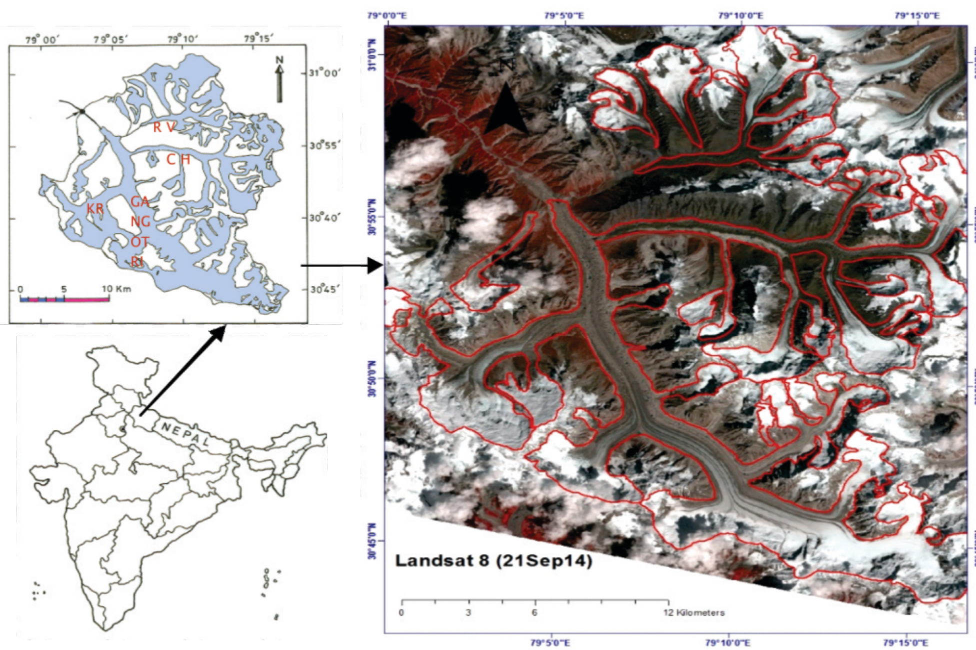

Figure 1 Location map and FCC image ofGangotri Group of Glacier

2. Experimental program

In the following section, the different ice volume estimation approaches applied in this study are described. Methodologies description are restricted to short summaries and background information can be studied from the given reference of the study.

2.1 *Area-related thickness estimations*

The most frequently used approach for ice volume estimations so far is V–A scaling method. As large glaciers generally tend to be thicker ice volume is calculated as a function of its surface area. Area-related scaling techniques have been extensively applied as their application is simple, fast and area data had been measured and compiled long before digital terrain information became available, hence a long term data is available. V–A scaling relation is generally represented as:

$$V=cA^{\gamma}$$

Where, V represents the glacier volume, A the glacier area, γ and c are two scaling parameters.
In order to facilitate comparisons with results from other methods and ice thickness measurements, Eq. (1) can be translated into the thickness–area relation as:

$$H=cA^{\beta} \quad (2)$$

Where, H represents the ice thickness and $\beta = \gamma$-1.
Here we use three sets of scaling parameters, applied in (Frey et al., 2014): (i) Chen and Ohmura (1990), (ii) Bahr et al. (1997), and (iii) LIGG et al. (1988). These parameters have been applied for the whole H-K range but a local study is the parameters and its accuracy is tested.The applied scaling parameters used in this study are given in Table 1.

Table 1 Parameter of the applied V-A relations

Source	C	γ
Chen and Ohmura (1990)	0.2055	1.36
Bahr et al. (1997)	0.191	1.375
LIGG et al., (1988)	0.8433	1.3

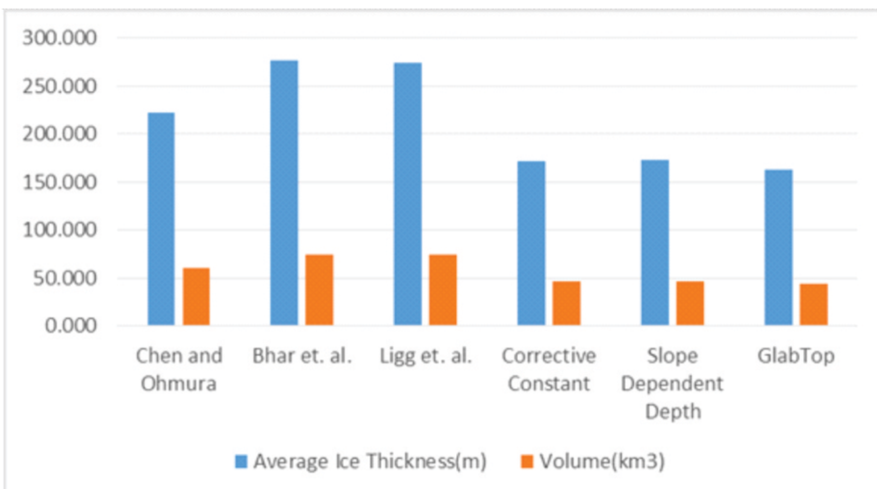

Figure 2 Comparative listing of results of the Study Note: Axis-y the in figure represents numerical value for both average ice thickness (denoted by m) and average total volume calculated from the relation (denoted by km^3).

A comparative list of the methods employed for ice depth is shown in Figure 2. As is clearly seen in the graph both GlabTop and slope dependent method are nearer to each other as expected. But other models using the old V-A (Volume-Area) scaling technique are constantly overestimating the mean glacier depth. When compared to velocity dependent Laminar flow based model, the mean depth drops to more than 20m at 92m.

Hence a corrective constant for Gangotri Glacier is suggested which are more in line to the results from other models. New factors based on studying the depth in this study are suggested for Gangotri group of glaciers for further V-A analysis in future is suggested as c = 0.193 and γ = 1.35.

2.2*Slope-dependent thickness estimations and GlabTop*

Haeberli and Hoelzle(1995) presented a way to estimate glacier volume using average surface slope and vertical glacier relief. This parameterization scheme has been used over Himalayan range in recent studies (Frey et al., 2014). Therefore, an application of this approach can be used for depth estimation over the study area.Here the equation governing the depth at center flow line of the glacier can be written as:

$$h\_centre = \tau / f \sigma g \sin\alpha \qquad (3)$$

The shape factor, f, is determined from (Cuffey and Paterson, 2010)

Table.2 Shape Factor for different glacier geometries

W		F	
	Parabola	Semi-ellipse	Rectangle
1	0.445	0.5	0.558
2	0.646	0.709	0.789
3	0.746	0.799	0.884
4	0.806	0.849	
8	1	1	1

Which is typically chose at 0.8 for valley glaciers. To interpolate the value at centre flow line over the whole of glacier taking the edges of the glacier to be at 0 ice depth, a multiplication of $\pi/4$ is applied.

$$h_G = h_{centre} \qquad (4)$$

The change in basal stress in accordance with elevation range is based on reconstructed latePleistocene glaciers of European Alps(Paul and Linsbauer, 2012). Where,

$$\tau = \begin{cases} 0.5 + 159.81\mathrm{H} - 43.5(\Delta H)^2, & \Delta H \leq 1.6km \\ 150 & \Delta H > 1.6km \end{cases} \qquad (5)$$

When applied over remotely sensed data, these parameters need to be considered for accurate determination. Hence ΔH (difference in height from snout to peak of glacier involved) and glacier length ⌊is used to determine slope of the glacier using the equation:

$$\alpha = \arctan(\Delta H/l) \quad (6)$$

This is then used to calculate the stress for the main glacier branch and consecutively centre flow line depth. This flow line depth is then interpolated to the glacier boundary which is fixed at zero depth using equation (4).

Paul and Linsbauer (2012)used an hybrid approach using inputs fromClarke et al., (2009) and Li et al., (2011), which considers just the flow dynamics and enables the bed estimation to be computationally very fast. The GlabTop model approach uses hydrological correct approach of digitizing flow-lines and takes into consideration the changes in τ every 500m, whereas slope dependant model does not consider variable τ but takes mean value for full glacier.

The DEM used for the study is converted into a contour line with 50 m elevation difference. This is then converted into slope map and equation (5) is applied to calculate the value of τ. This is then used to calculate the ice depth distribution along the flow lines which are digitized earlier following the contour lines. The TopoToRaster tool is used from the ArcGIS to interpolate the values of the ice depth over the entire glacier from the flow line to the entire glacier.

2.3 *Ice Thickness from velocity measurement*

2.3.1 *Velocity Measurement*

Surface velocities of the glacier were calculated using sub-pixel correlation of the acquired multi temporal images, using the ENVI module Co-registration of Optically Sensed Images and Correlation (COSI-Corr), which is downloadable at http://www.tectonics.caltech.edu/. The algorithm uses two images to iteratively cross-correlate in the phase plane on sliding windows, to find the best possible correlation. A detailed description of the algorithm is given by (Leprince et al., 2007). The setup provides alteration of the window size, window movement, signal to noise ratio threshold and gridded output options. The setting of these depend on the expected movement of the glacier and the pixel resolution of the image. Table 2. Provides us with the setting used in the velocities measurements. All pixels that have SNR < 0.9 and displacements >85m are discarded. A vector field is generated from the two displacement images and is then overlaid on the image to check the accuracy of the measurement. The difference in the time of acquisition between the two images is used to estimate the velocity field.

$$D_{s=\sqrt{(E-S^2)+(N-S^2)}} \quad (7)$$

Where, D represent the translation movement detected, E-S represent the movement values for the E-S direction and N-S represent the movement values for the N-S direction. Although care has to be taken to disregard all pixel having SNR less than 0.9, hence leaving patches of area with no movement values. This is then rectified by interpolating nearby values. Velocity calculation is then a simple matter of movement divided by the time interval between the two scenes. This is done using vector addition of the two fields of movement with the angle between them always at 90°. This is used to get the magnitude of the movement of the feature over the search window. Also local averaging is done to filter out rouge pixel showing movement values very high which are obviously termed as noise.

Table 3 COSI-Corr Settings used in the study

Window Size		Resolution (m)	Step	Robustness Iteration	Mask Threshold
Initial	Final				
64	32	15	2	4	0.9
128	64	15	2	4	0.9
256	64	5	2	4	0.9
256	128	5	2	4	0.9
512	256	5	2	4	0.9

2.3.2*Estimation of Depth*

Ice thickness calculation are done using velocity values derived from the COSI-CORR software. The basic premise behind the model for thickness estimation follows the logic of Basal Shear stress and Velocities in "Laminar flow" as described in (Cuffey and Patterson, 2010). Here the model of a glacier is a parallel-sided slab of ice of thickness H on a rough plane of slope α. No sliding of the slab is assumed on the plane and the thickness of the slab is much less than its length and width. The slab is perpendicular to the plane and of unit cross section. The weight of the slab is ρgH. Where ρ is density of ice, g is acceleration due to gravity and H is the height of the slab. The weight of the slab along the surface will be countered by basal stress which will be equal to:

$$\tau_b = \rho g H sin\alpha \quad (8)$$

This is a very simple model for glacier movement when the layers of ice do not move over each other. But in real world scenarios, ice moves over each layer and hence velocity varies with depth. This is shown in Figure 1. Here a block of ice is taken with unit length at all sides. This give rise to the premise that these blocks of ice move over each other hence producing sliding motion.

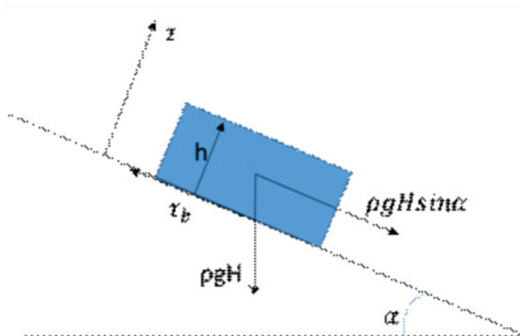

Figure 3 Forces acting on a block of ice

Let u be the x component of the velocity. Assuming the slab deforms in a simple shear, the flow lines are parallel to surface. This is Laminar flow of ice. It follows that the z component of the velocity is zero and so shear strain rate is ½(du/dz).

$$\frac{1}{2}\frac{du}{dz} = A\tau_b^n \qquad (9)$$

Where, A is a creep parameter (which depends on temperature,fabric, grain size and impurity content and has a value of$3.24*10^{-24}$ Pa^{-3} s^{-1} for temperate glaciers (Cuffey and Paterson, 2010).Using equation (8) and adding a scale/shape factor, f, for temperate glaciers we get

$$\tau_b = f\rho g(h-z)sin\alpha \qquad (10)$$

Integrating equation (9) into (8) we get

$$u_s - u(z) = \frac{2A}{n+1}(f\rho gsin\alpha)^n(h-z)^{n+1}$$

(11)

This equation can then be used to determine the depth/height of the ice over any glacier where our assumption holds true. Changing the equation into the final form by replacing (h-z) with H we get.

$$u_s - u_b = \frac{2A}{n+1}(f\rho gsin\alpha)^n(H)^{n+1}$$

(12)

Rearranging to get depth information of a particular velocity pair, we get:

$$H = \sqrt[n+1]{\frac{(n+1)(u_s - u_b)}{2A(f\rho g sin\alpha)^n}} \qquad (13)$$

Where, f is a scale factor, i.e. the ratiobetween the driving stress and basal stress along a glacier, and has a range of [0.8, 1] for temperate glaciers. This study has used f = 0.8 (Haeberli and Hoelzle, 1995), ρ is the ice density, assigned a constant value of900 kgm^{-3} (Farinotti and others, 2009a), g is accelerationdue to gravity (9.8ms^{-2}) and Slope,

Table 4 Slope Dependent Model Parameters and Results

Name	Length (km)	ΔH(km)	Slope (rad)	τ	Ice depth (m)	Area Covered (km^2)
Gangotri	30	3.2	0.10626	150	200.42	87.87
Raktvarn	10.27	2	0.19233	150	111.21	47.88
Chaturangi	15.18	1.2	0.07888	129.62	233.10	64.89
Swachand	6.81	1.15	0.16729	126.7413	107.87	16.11
Malandi	4.26	0.85	0.19694	104.9013	75.97	4.58
Meru	8.53	1.45	0.16837	140.7513	119.03	5.57
Kirti	9.01	2	0.21843	150	98.10	31.60
Ghanohim	4.03	0.6	0.14779	80.72	77.68	11.83

The Ice depth is the most in the main trunk and Chaturangi glacier at 222.10m and 233.10m respectively. These are also some of the largest spanning glaciers in the group. This supports the hypothesis that states the depth as directly proportional to its area. All other glacier branches are medium in depth (75.97m to 119.03m) with the average depth and volume calculated to be 172.88m and 46.7376$km^3$for the whole glacier.

Table 5 Slope Dependent Model Parameters and Results

Name	Length (km)	ΔH (km)	α(rad)	τ	Ice depth (m)	Area Covered (km^2)
Gangotri	30	3.2	0.10626	150	200.42	68.4
Raktvarn	10.27	2	0.19233	150	111.21	47.88

Swachand	15.18	1.2	0.07888	129.62	233.10	64.89
Swachand	6.81	1.15	0.16729	126.7413	107.87	16.11
Malandi	4.26	0.85	0.19694	104.9013	75.97	4.58
Meru	8.53	1.45	0.16837	140.7513	119.03	5.57
Kirti	9.01	2	0.21843	150	98.10	31.60
Ghanohim	4.03	0.6	0.14779	80.72	77.68	11.83
Gangotri2	4.7	1	0.20963	116.8	79.54	19.47

GlabTop model (Paul and Linsbauer, 2012) uses the same technique as defined for slope dependent approach but depth calculation are done for height intervals. This means that the branch lines digitized are more intensive and conform to the hydrological structure of the glacier bed. Hence τ, basal sheer stress, is calculated for height interval of 500m each. This allows for more flexibility in calculating ice depth or bed topography of complex glacier system like Gangotri.

Table 6 provide velocity measurement from the COSI-Corr parameterization used in the Table 3 for all the image pairs used in the study. This includes both medium and high resolution images.

Table 6 Velocity measurement from COSI-Corr for related image pairs

Satellite	Date Pair	Window Size		Resolution (m)	Movement		SNR	Time	Velocity
		Initial	Final		E-W	N-S		Interval	(m/day)
Landsat 7	9Sep98-22Oct99	64	32	15	9.974	6.22	0.9	408	0.0288
Landsat 7	8Oct00-20Oct01	64	32	15	8.89	6.812	0.9	377	0.0297
Landsat 7	22Oct99-8Oct00	64	32	15	4.893	3.59	0.9	352	0.0172
Landsat 7	20Oct01-8Jun02	64	32	15	6.172	7.04	0.9	231	0.0405
Landsat 7	22Oct99-20Oct01	128	64	15	14.183	10.188	0.9	729	0.0239
Landsat 7	8Oct00-28Aug02	128	64	15	8.511	10.638	0.9	689	0.0197
Landsat 7	9Sep98-8Oct00	128	64	15	10.389	8.46	0.9	760	0.0176
Landsat 8	26Aug13-21Sep14	64	32	15	5.396	6.509	0.9	391	0.0216
IRS	22Oct00-08Jul02	256	64	5	6.889	7.323	0.9	624	0.0161
IRS	22Oct00-05Oct03	256	64	5	7.554	8.215	0.9	1078	0.0103

IRS	8Jul02-20Oct05	256	64		5	5.968	5.609	0.9	1200	0.0068
IRS	8Jul02-5Oct03	128	32		5	7.902	7.281	0.9	454	0.0236
IRS	5Oct03-20Oct05	256	64		5	5.553	5.491	0.9	746	0.0104

The average velocity for the period of observation from 9 September 1998 to 21 September 2014 was calculated to be 0.02 m day^{-1}for whole glacier. This observation when limited to upper areas of the observation yielded an average movement of 0.041 m day^{-1}.This observation when limited to upper areas of the observation yielded an average movement of 0.041 m day-1. Velocity from earlier reported papers varies from 0.038–0.233 m day–1 in the accumulation region to 0.055–0.0821 m day–1 near the snout (Gantayat et al., 2014). Kumar et. al., (2008) reported Gangotri glacier retreat using rapid static and kinematic GPS survey to be in range of 0.033-0.0376 mday-1 (during 2004-2005). Saraswat et al. (2013) showed that Gangotri glacier snout has receded at a rate of 21.3 ± 3 myear−1 (0.058 mday-1) over a period of 6 years (2004–2010). Further, the average glacier surface velocity in the northern (lower) portions (28.1 ± 2.3 m year−1 or 0.077 mday-1) is observed to be significantly lower than in the southern (higher) portions (48.1 ± 2.3 m year−1 or 0.13 mday-1) of the Gangotri glacier.

Figure 4 Velocity Vectors over Gangotri Glacier

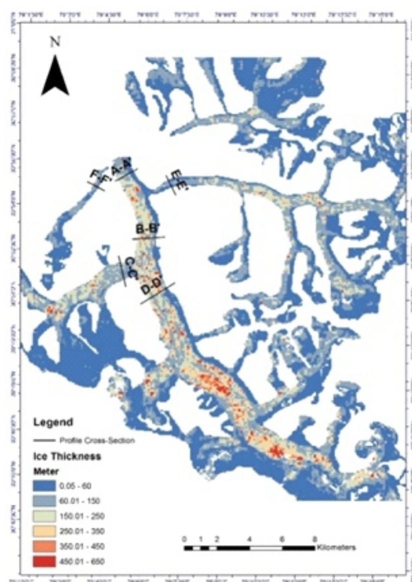

Figure 5 Mean Ice Depth Profile of Gangotri Glacier from time of analysis (1998-2014).

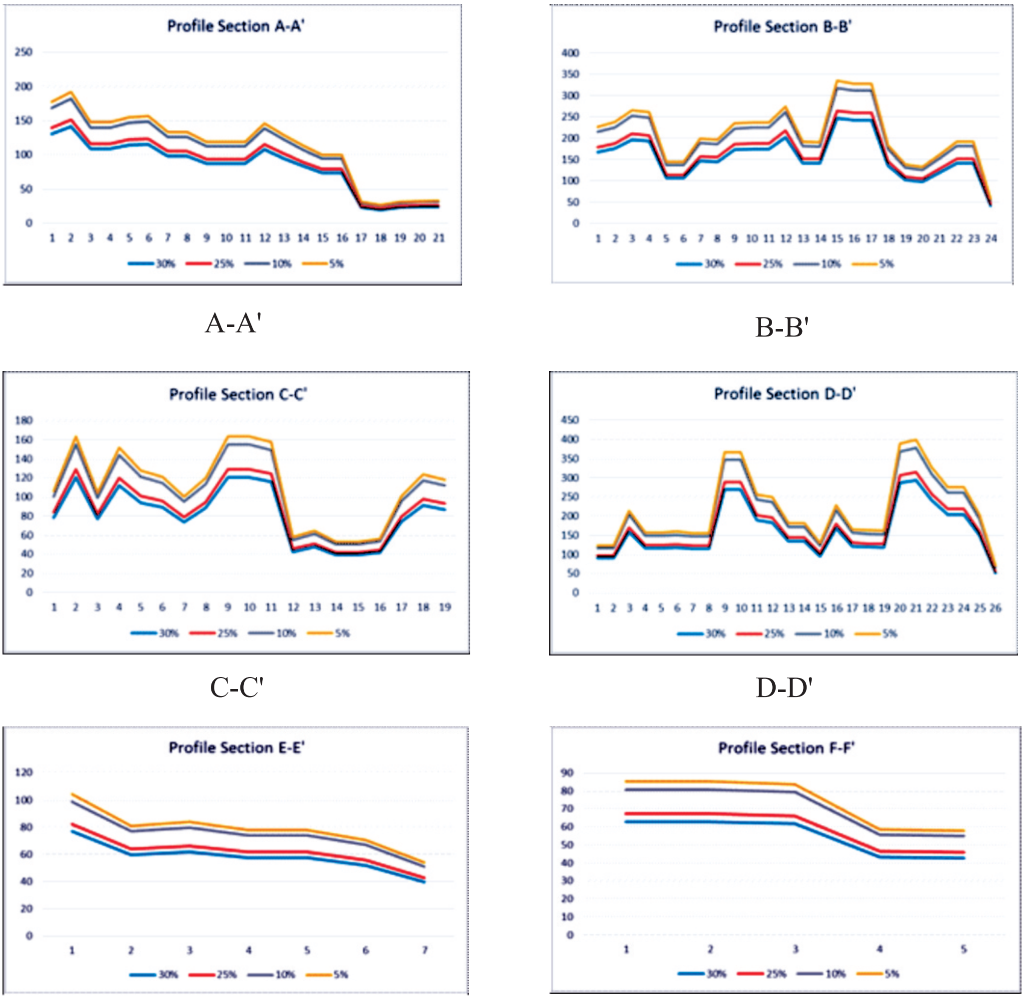

A-A' B-B'

C-C' D-D'

E-E' F-F'

Figure 6 Profile cross-Section for different ratio of basal velocity(in terms of percentage of surface velocity) Note: (A-F) x-axis represent the profile length (100m interval) from x-x'; y-axis represents ice thickness calculated from the model.

The major conclusion of the profile analysis have shown that the variation in Lamiar flow model is very huge where variation from 20m to 400m is easily visible. Also the depth at snout was found to be ~60 m and the maximum depth was found at accuumulation zone at ~650 m. Uncertainty analysis procedure wassimilar to as reported in (Gantayat et al., 2014). In present study, velocity uncertaintyon snow free ground for IRS 1C/1D is in range of 0 to 0.351 m and a maximum of 1.5 m. Values for uncertainty of surface velocity was fixed at 3.5 m $annum^{-1}$ based on observed values by (Swaroop et. al., 2003). Scaling factor uncertainty was set at 0.1 (Gantayat et al., 2014). Creep factor uncertainty was set at $8.24*10^{25}$ (Farinotti et al., 2009a). Uncertainty over ice density accuracy is taken at 90 kgm^{-3} i.e. 10% of the defined density used in the study. Uncertainty in the slope estimation using SRTM DEM is calculated to be at 0.001. All the reported uncertainty are then added for uncertainty in the volume estimation of the Glacier which is reported to be 11.4% for the current study. A marked decrease of uncertainty by 7% from earlier reported study (Gantayat*et. al.,* 2014). This is possible due to use of high resolution imagery (5 to 15m as compared to 30 m) (Farinotti*et. al.,* 2009) used for velocity estimation and better vertical relative accuracy achieved from STRM DEM (± 10 m) as compared to ASTER GDEM(± 20 m).

4 Validation and discussions

Ice thickness was validated by TLS measurement at snout for 9 Points. These were kept at a distance of 30 m to 100 m apart from each other. The scan of the area was taken and overlaid over the model output. This is then used to measure the thickness of the ice from a stone visible in the scan and detached from the main glacier, lying in the river bed. This stone was used as reference for the thickness measurement which varied from 58 m to 67 m at snout validating the model estimation of ice thickness at ~60 m.Gantayat*et. al.,* (2014) reported the maximum ice thickness as 540 m to 50–60 m as minimum at snout. This is slightly different from present study, where minimum ice thickness at snout is estimated as 60 – 67 m and 650 m as maximum ice thickness. This difference can be attributed to different data source with high resolution data such as IRS 1C/1D Pan Data and 90 m SRTM DEM based slope.

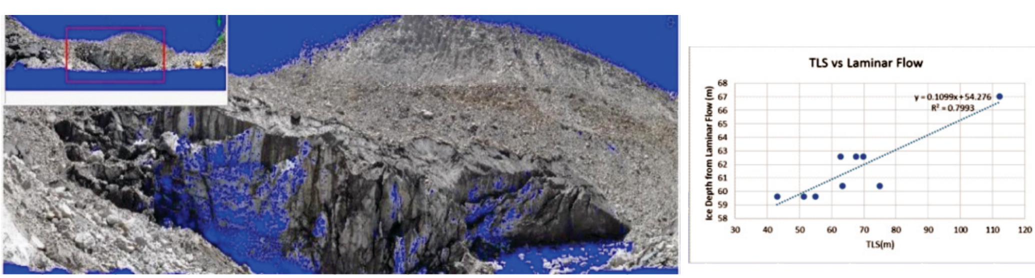

Figure 7 Correlation between TLS ground Measurements and Laminar Flow Model at snout and the Actual Scan of the snout during field visit (15-17 September 2014)

Frey et al., 2014 has reported an average ice depth as 145 m for GlabTop2 Model and 91 m for Slopedependent thickness estimate. The study concludes the average thickness of the Gangotri Glacier to be 92.25 m which is close to the reported value by (Frey et al., 2014). Future work can include use of Ground Penetrating Radar (GPR) for depth measurement and validation of the ice thickness for whole glacier. Field survey using DGPS can be done to validate surface velocity of the glacier. Parameterization of the laminar flow model for density, scaling factor, creep factor, and basal velocity can be further studied for better results.

Acknowledgement:

Authors express their sincere thanks to Director IIRS, A Senthil Kumar and former Director YVN Krishnamurthy for their constant support encouragement and all institutional facilities to complete this work. Thanks are also due for Head and faculty of Photogrammetry and Remote Sensing Department (PRSD) for providing and training of TLS and DGPS operations used in field survey, CMD IIRS and VSSC Trivandrum Engineers to provide solar panels and fuel cell based instrument charging systems, Forest Department Uttarakhand and SASE Chandigarh for giving permission to visit Gangotri glacier and stay at Bhojbasa, NRSC Data Centre (NDC) and USGS for providing satellite data used in this study.

References

1. Bahr, D. B., Meier, M. F., and Peckham, S. D.: The physical basisof glacier volume–area scaling, J. Geophys. Res.-Solid, 102,20355–20362, 1997.
2. Bolch, T., Kulkarni, A., Kääb, A., Huggel, C., Paul, F., Cogley, J.G., Frey, H., Kargel, J. S., Fujita, K., Scheel, M., Bajracharya,S., and Stoffel, M.: The State and Fate of Himalayan Glaciers,Science, 336, 310–314, doi:10.1126/science.1215828, 2012.
3. Chen, J. and Ohmura, A.: Estimation of Alpine glacier water resourcesand their change since the 1870s, IAHS Publications –Hydrology in Mountainous Regions, I – Hydrological Measurements;the water cycle, Proceedings of two Lausanne Symposia,August 1990, edited by: Lang, H. and Musy, A., IAHS Publ.,193, 127–135, 1990.
4. Clarke, G., Anslow, F., Jarosch, A., Radic, V., Menounos, B., Bolch, T., and Berthier, E.: Ice volume and subglacial topography for western Canadian glaciers from mass balance fields, thinning rates, and a bed stress model. J. Climate, 26, 4282–4303, doi:10.1175/JCLI-D-12-00513.1, 2013.

5. Cuffey, K.M., Paterson, W.S.B., 2010. The Physics of Glaciers. Elsevier Science.
6. Farinotti, D. and Huss, M.: An upper-bound estimate for the accuracy of glacier volume–area scaling, The Cryosphere, 7, 1707– 1720, doi: 10.5194/tc-7-1707-2013, 2013.
7. Farinotti, D., Huss, M., Bauder, A., Funk, M., and Truffer, M.: A method to estimate the ice volume and ice-thickness distribution of alpine glaciers, J. Glaciol., 55, 422–430, 2009.
8. Farinotti D, Huss M, Bauder A, Funk M and Truffer M. A method to estimate ice volume and ice-thickness distribution of alpine glaciers. J. Glaciol., 55(191), 422–430, doi: 10.3189/ 002214309788816759, 2009a.
9. Farinotti D, Huss M, Bauder A and Funk M. An estimate of the glacier ice volume in the Swiss Alps. Global Planet. Change, 68(3), 225–231, doi: 10.1016/j.gloplacha.2009.05.004, 2009b.
10. Frey, H., Machguth, H., Huss, M., Huggel, C., Bajracharya, S., Bolch, T., Kulkarni, A., Linsbauer, A., Salzmann, N., Stoffel, M. Estimating the volume of glaciers in the Himalayan-Karakoram region using different methods. The Cryosphere 8, 2313–2333. doi:10.5194/tc-8-2313-2014, 2014
11. Gabbi, J., Farinotti, D., Bauder, A., and Maurer, H.: Ice volume distribution and implications on runoff projections in a glacierized catchment, Hydrol. Earth Syst. Sci., 16, 4543–4556, doi: 10.5194/hess-16-4543-2012, 2012.
12. Gantayat, P., Kulkarni, A. V., and Srinivasan, J., Estimation of ice thickness using surface velocities and slope: case study at Gangotri Glacier, India, Journal Of Glaciology, Vol. 60, No. 220, doi: 10.3189/2014JoG13J078, 2014.
13. Gardner, A. S., Moholdt, G., Cogley, J. G., Wouters, B., Arendt, A. A., Wahr, J., Berthier, E., Hock, R., Pfeffer, W. T., Kaser, G., Ligtenberg, S.
14. R. M., Bolch, T., Sharp, M. J., Hagen, J. O., Van den Broeke, M. R., and Paul, F.: A Reconciled Estimate of Glacier Contributions to Sea Level Rise: 2003 to 2009, Science, 340, 852–857, doi:10.1126/science.1234532, 2013.
15. Glen, J. W.: The Creep of Polycrystalline Ice, P. Roy. Soc. A, 228, 519–538, doi:10.1098/rspa.1955.0066, 1955.
16. Haeberli,W. and Hoelzle, M.: Application of inventory data for estimating characteristics of and regional climate-change effects on mountain glaciers: a pilot study with the European Alps, Ann. Glaciol., 21, 206–212, 1995.
17. Huss, M. and Farinotti, D.: Distributed ice thickness and volume of all glaciers around the globe, J. Geophys. Res., 117, F04010, doi: 10.1029/2012JF002523, 2012.
18. Huss, M., Farinotti, D., and Bauder, A.: Modelling runoff from highly glacierized alpine drainage basins in a changing climate, Hydrol. Process. 22, 3888–3902,

doi:10.1002/hyp.7055, 2008.
19. Immerzeel, W. W., van Beek, L. P. H., and Bierkens, M. F. P.: Climate Change Will Affect the Asian Water Towers, Science, 328, 1382–1385, doi:10.1126/science.1183188, 2010.
20. Jacob, T., Wahr, J., Pfeffer, W. T., and Swenson, S.: Recent contributions of glaciers and ice caps to sea level rise, Nature, 482, 514–518, doi:10.1038/nature10847, 2012.
21. Jain SK (2008) Impact of retreat of Gangotri glacier on the flow of Ganga River. Current Sci., 95(8), 1012–1014
22. Kääb, A., Berthier, E., Nuth, C., Gardelle, J., and Arnaud, Y.: Contrasting patterns of early twenty-first-century glacier mass change in the Himalayas, Nature, 488, 495–498, doi: 10.1038/nature11324, 2012.
23. Kamb, B. and Echelmeyer, K.: Stress-gradient coupling in glacier flow, I: Longitudinal averaging of the influence of ice thickness and surface slope, J. Glaciol., 32, 267–284, 1986.
24. Kaser, G., Grosshauser, M., and Marzeion, B.: Contribution potential of glaciers to water availability in different climate regimes, P. Natl. Acad. Sci. USA, 107, 20233–20227, doi:10.1073/pnas.1008162107, 2010.
25. Leprince S, Barbot S, Ayoub F and Avouac J-P (2007) Automatic and precise orthorectification, coregistration, and subpixel correlation of satellite images, application to ground deformation measurements. IEEE Trans. Geosci. Remote Sens., 45(6), 1529– 1558 (doi: 10.1109/TGRS.2006.888937).
26. Li, H., Ng, F., Li, Z., Qin, D., and Cheng, G.: An extended "perfect-plasticity" method for estimating ice thickness along the flow line of mountain glaciers, J. Geophys. Res., 117, F01020, doi: 10.1029/2011JF002104, 2011.
27. Linsbauer, A., Paul, F., Hoelzle, M., Frey, H., and Haeberli, W.: The Swiss Alps without Glaciers – A GIS-based Modelling Approach for Reconstruction of Glacier Beds, in: Proceedings of Geomorphometry 2009, edited by: Purves, R., Gruber, S., Straumann, R., and Hengl, T., University of Zurich, Zurich, 243–247, 2009.
28. LIGG, WECS, and NEA: Report on first expedition to glaciers and glacier lakes in the Pumqu (Arun) and Poiqu (Bhote-Sun Kosi) river basins, Xizang (Tibet), China, Science Press, Beijing, China, 1988.
29. McNabb, R. W., Hock, R., O'Neel, S., Rasmussen, L. A., Ahn, Y., Braun, M., Conway, H., Herreid, S., Joughin, I., Pfeffer, W. T., Smith, B. E., and Truffer, M.: Using surface velocities to calculate ice thickness and bed topography: a case study at Columbia Glacier, Alaska, USA, J. Glaciol., 58, 1151–1164, 2012.
30. Frey, H., Machguth, H., Huss, M., Huggel, C., Bajracharya, S., Bolch, T., Kulkarni, A., Linsbauer, A., Salzmann, N., Stoffel, M., 2014. Estimating the volume of glaciers in the Himalayan–Karakoram

region using different methods. The Cryosphere 8, 2313–2333. doi:10.5194/tc-8-2313-2014

31. Paul, F., Linsbauer, A., 2012. Modeling of glacier bed topography from glacier outlines, central branch lines, and a DEM. Int. J. Geogr. Inf. Sci. 26, 1173–1190. doi:10.1080/13658816.2011.627859

Radi´c, V. and Hock, R.: Regional and global volumes of glaciers derived from statistical upscaling of glacier inventory data, J. Geophys. Res., 115, F01010, doi:10.1029/2009JF001373, 2010.

32. Saraswat, P., Syed,T.H., Famiglietti, J.S., Fielding, E.J., Crippen, R. Gupta, N. Recent changes in the snout position and surface velocity of 592 Gangotri glacier observed from space. International Journal of Remote Sensing, 34:24, 8653-8668, doi: 10.1080/01431161.2013.845923, 2013.

33. Swaroop S, Raina VK and Sangeswar CV (2003) Ice flow of Gangotri glacier. In Srivastava D, Gupta KR and Mukerji S eds. Proceedings of the Workshop on Gangotri glacier, 26–28 March 2003, Lucknow, India. (Spec. Publ. 80) Geological Survey of India, Kolkataata

PROBABLE CAUSES OF FAILURE OF EXISTING EMBANKMENTS AT SUNDARBAN – A PRELIMINARY STUDY

Gupinath Bhandari (Associate Professor)

Department of Civil Engineering, Jadavpur University, Kolkata 700032, INDIA

E-mail: g.bhandari@civil.jdvu.ac.in

Abstract:

The recurring failure of earthen/ brick pitched embankments especially during monsoon at some islands of Sundarban resulting the inundation and saline water intrusion to the agriculture field. Addressing to this problem needs a holistic approach including geotechnical investigation, embankment stability analysis, river hydrodynamic analysis, tidal hydraulic study, coastal dynamics study and sediment budgeting. A preliminary study has been attempted considering embankment stability, seepage and drawdown.

Background

A total length of 3520km marginal embankment exists all around Sundarban on either side of the existing creeks in the estuarine system. Since these embankments were not constructed in a scientific or engineered manner, failure of the same became a routine in this area. As revealed from the history of failure, it occurs especially during monsoon and storm surges. Out of the total length, about 434 km stretch of embankment appears to be vulnerable.

Geological and geomorphologic setup of the study area

The Sundarban island system is geologically very recent. The Delta outbuilding of Ganga-Brahmaputra system though initiated at the end of Miocene, could have reached the present location of Sundarban delta, not more than 10,000 years back

(Pleistocene to Recent). The geological formation covering the island system belongs to the 'Bengal Alluvium'.

During the recent times the Bengal delta acquired a typical tide dominated lobate form with a tidal range of 3.7 to 5m. The estuarine mouth of Hoogly and its numerous distributaries like Saptamukhi, Jamira etc. acquired a typical seaward flaring funnel shaped pattern. Due to progressive upliftment of channel bed, the height of tidal bore became maximum 6.4m and further inland this increased to 7.17m as obtained Tide Table of Hoogly River, published by Kolkata Port Trust, 1984 (the then Calcutta Port Trust). The flood and ebb tides have a semi-diurnal nature (12.5 hours interval) and occur twice daily. Within this cycle floodwater flows for 2-3 hours duration. At the remaining 8-9 hours, the estuary is covered by ebb tide flow of lesser velocity.

Physical setup of the study area

Sunderban is complicated delta formation consists of a network of a number of creeks and which divide the entire area into large number of islands, under the area of Hooghly-Matla estuarine system. These channels and creeks meet to the Bay of Bengal through the entire estuarine system.

Topography: The general topography of Sunderban is the immature fertile islands, which were built by the alluvial silt carried by Ganga and other rivers.

River System: The whole of the Sunderban is comprised of intricate network of criss-cross channels and which divide the entire area into a large number of islands, these channels and creeks ultimately find their way to the Bay of Bengal through some principal estuaries. These rivers are Hoogly, Muriganga, Saptamukhi, Thakuran, Matla, Gosba, Haribhanga and Raimangal.

Role of Tide: Tides used to play a vital role, before construction of embankment, in deltaic building process in the Sundarban. Due to continuous effect of flood tide and ebb tide twice a day, the silt carried down by the river get deposited in layers, after construction of embankments, at the confluence of rivers, which in tern rise the bed level and reduce the navigability. The tidal variation in this region is about 4m and above. Sometimes the higher tides generate the tidal surge on the embankments.

Problems At Study Area

It is said that entire area of Sunderban was under forest before British rule. Some private entrepreneurs, being attracted by fertility of land and considering the proximity of Kolkata, started premature reclamation of the north-west area of Sunderban in and around 1770, under the patronage of the East India Company, by denudation of forest and putting marginal embankment along the periphery of a large number of islands to protect the low laying area from tidal inundation. The evil effect of such unfair and unwise human interference in Sundarban started from that very day, and subsequently such premature reclamation spreaded over the entire Sunderban and continued upto 1909, when the British Government enforced an act on controlling further reclamation of new areas. The construction of marginal embankment around the island created the problem of drainage of the related area during monsoon and cuts in the embankment were resorted for effective drainage, such cuts often led to breach in the embankment during spring tide or tidal surges. The construction of embankments also results the problem related to silt deposition, which was carried by the rivers, especially during flood tide. Earlier, before construction of marginal embankment, the low laying islands were usually flooded with the seawater/ mixed water containing high silt, during flood tide, which was the driving factor to mature the islands of Sundarban. But after construction of marginal embankments it was just stopped and the silt was being started to deposit on the riverbed itself, resulting the reduction of navigability of the channels/ creeks and the tidal flood around Sundarban. This fact might have accelerated the disaster of breach out of embankments around this area.

General Condition of Existing Embankments

As revealed from the available reports, a part of the total length is purely earthen embankments, while the others are either brick pitched or boulder pitched. The vulnerable stretches may be seen at the brick/ boulder pitched embankments (Plate 1a), as well as only earthen embankments (Plate 1b).

 

Plate 1: Distressed (a) Brick Pitched (L) and (b) Earthen Embankment (R)

These embankments are experiencing different hydrodynamic condition at different places. The hydrodynamic condition may be direct coastal dynamics, different tidal dynamics or meandering dynamics. Out of the total length, only 12% is vulnerable as reported elsewhere, but the area under this portion get inundated during monsoon, which causes the saline water intrusion in the agriculture field and habitable area causing disaster to the local people.

The several field visits reveal that the geometrical parameters, such as height and slope, of the embankments were varying, that might be as per the local site condition including hydraulic condition, while the soil properties of the embankment body do not varying much.

Formulation Of The Present Study

The marginal embankments, which were constructed around Sundarban estuarine system at premature stage of the island system, are facing severe problem of erosion. The construction was carried out using locally available soil with different arbitrary profiles, without detailed study of the engineering properties of the soil used and the stability analysis of the slopes of the embankments. The erosion or breach out of embankments is occurring regularly specially during monsoon or storm surges.

The fluctuation of water level in the creeks due to tidal cycle, including diurnal changes, may develop the pore pressure in the embankment body. During the extreme events of storm surges, the water column might be observed as in the order of 5-6m height, which hits the embankment, and causes the spill over of the same.

The present study was formulated, in the light of the earlier discussion in previous paragraphs, to carry out the slope stability analysis of embankments, considering the existing subsoil and embankments soil properties and seepage, also the horizontal sliding stability of the embankments for tidal variation, considering the draw down condition and seepage. The analysis incorporates (Das and Bhandari, 2005) different geometrical dimension of the embankments and hydraulic forces at the existing soil condition. The height of the embankments considered in the study 2.0m to 4.0m with the increment of 0.5m, while the slopes were taken 1:1, 1:1.5, 1:2 and 1:2.5 (H:V). The variation of hydraulic condition was considered through freeboard ranges between 0.0m to 1.00m with an increment of 0.25m in case of horizontal sliding analysis, while the values of pore pressure coefficient were taken 0.3, 0.4 and 0.5 for slope stability analysis in consideration with the existing soil condition as clayey silt.

Geotechnical Investigation

Since the subsoil properties could not be made available, the subsoil investigation for stability analysis of the existing embankments was essential for the present study. Three different locations were selected for this purpose.

Subsoil exploration

A subsoil investigation of the study area was essential for understanding the engineering properties of subsoil and embankment soil, which was for the stability analysis of existing embankments. Three boreholes were advanced at three locations of Sundarban, where the existing embankments are in distressed condition. Out of the three boreholes, two of them were advanced upto 10m each below ground level, while 6.5m could be advanced for the third one.

Choice of site

A large number of locations may be available in Sundarban, where the existing embankments are in distressed condition. A detailed soil investigation of all the vulnerable stretches is necessary for proper understanding of the problem. But to get access to those places are either difficult or prohibitive; hence the mobilisation of soil investigation equipments is very difficult. In the present study to initiate the work, three locations; Sonakhali (N22°12'31.5”, E88 ° 42'27.6”), Napitkhali (N22°13.33'33”, E88°44'43.7”) and Choravidya (N22 ° 19'25.9”, E88°48'27.3”) were selected (Figure 1). The selected places are well connected to Kolkata by road transport and the existing embankments at these places are in distressed condition as well. Two boreholes of 10m depth below ground level each was advanced at Sonakhali and Napitkhali, one at each location, while at Choravidya the borehole was advanced only upto 6.5m due to non accessibility of the site.

More number of sites, where existing embankments are in vulnerable condition, has to be selected for detailed work on this problem for proper understanding of the soil properties of Sundarban area.

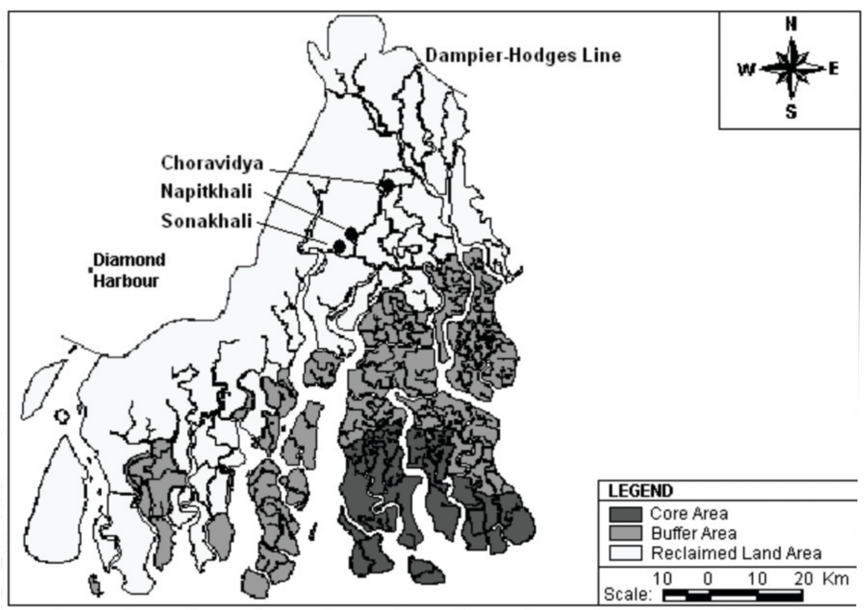

Figure 1: Map of Sundarban and Borehole Locations

Methodology of subsoil exploration

In the present study two methods; augur boring and wash boring was adopted for advancement of three boreholes at three different locations. In each case the borehole depth upto 6.5 below ground level was advanced by augur boring method using 300mm dia augur. The remaining depth upto 10m below ground level was advanced by wash boring technique, for all the cases. Precautions were taken to get the proper undisturbed soil samples. In wash boring no bentonite slurry was used. Undisturbed samples were collected, where the changes in strata were found through standard penetration tests during augur boring and/ or colour and silt content in case of wash boring. Standard penetration tests were conducted at an interval of 1.5m. However, the same could not be conducted at the depth where undisturbed samples were collected.

Undisturbed soil samples were also collected from embankment body at each of the three locations. At the three locations two undisturbed soil samples from each site were collected. Total six numbers undisturbed soil samples were collected from the embankment body to determine the engineering properties and the stability analysis.

Stratigraphy of subsoil

The stratification of subsoil of the selected area of Sundarban is almost similar as revealed from the subsoil investigation of three different locations. The general stratigraphy of the selected area is of three layers. The average stratigraphy as obtained has been presented in Figure 2. The top layer ranges between 0 and 1.5m depth below ground level has been obtained as brownish silty clay with decomposed wood, the second layer ranges between 1.5m and 6.0m depth below ground level has been obtained as gray silty clay, while the third layer ranges between 6.0m and 10.0m depth below ground level has been obtained as stiff gray silty clay, with traces of mica.

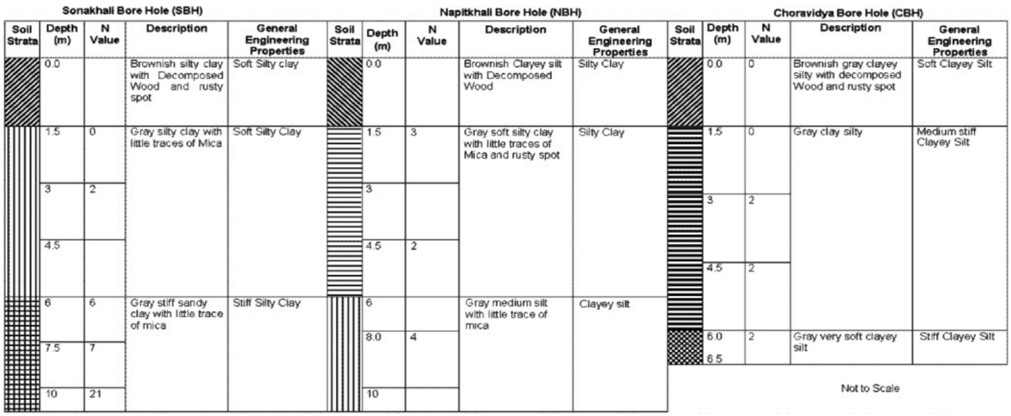

Figure 2: Bore Log Data Sheets of Sonakhali, Napitkhali and Choravidya

obtained as brownish silty clay with decomposed wood, the second layer ranges between 1.5m and 6.0m depth below ground level has been obtained as gray silty clay, while the third layer ranges between 6.0m and 10.0m depth below ground level has been obtained as stiff gray silty clay, with traces of mica.

Engineering properties of subsoil and embankment soil

Disturbed and undisturbed soil samples were collected from distressed embankment body and the subsoil.

The laboratory test has been carried out for the collected disturbed and undisturbed soil samples, to find out the engineering properties, specially the shear strength and permeability, of subsoil and the existing embankment soil prevailing at the selected sites. The average value of geotechnical data at different depth of the subsoil and embankment soil has been presented in Table 1, which was also considered for the analysis.

Subsoil						
Depth (m)		Shear Strength Parameters				Bulk density (γ) (t/m^3)
From	To	C (t/m^2)	ϕ	C′ (t/m^2)	ϕ'	
0.0	1.5	2.30	10.50	2.01	13.00	1.87

1.5	6.0	1.89	10.80	1.70	13.60	1.99
6.0	10	2.12	9.83	1.83	12.54	1.88
Embankment Soil						
-	-	1.90	6.50	1.97	9.63	1.87

Table 1: Geotechnical Data Adopted in the Stability Analysis

Method of Analysis

The stability of Sundarban embankments has been carried out in the present study primarily in two methods, which cover: (1) slope stability analysis in total stress condition and effective stress condition with different pore pressure coefficient, and (2) horizontal shear stability analysis at upstream and downstream side due to sudden drawdown and seepage respectively, assuming different freeboard condition. Seepage analysis has been carried out in the light of available theories suggested by Dvinhoff, and Harr (1971); Desai, and Sherman (1971); Desai (1972).

A computer programme has been developed in the present study. The programme used in the slope stability analysis is capable of handling any slope geometry. It can cater any number of soil layers, considers the effect of ground water table or phreatic line that may be present. Moreover, the programme can tackle four cases namely total stress analysis, effective stress analysis, total stress earthquake analysis and effective stress earthquake analysis respectively; though the earthquake analysis has not been considered in the present study due to low heights of the embankments. The programme also considers the effect any surcharge load, if present in the site. The programme uses the term the pore water pressure ratio, while considering the effect of water table and phreatic line and calculates the weights of the slices accordingly. The convergence rate, while doing the iterative calculations is rapid. The final value of the factor of safety is determined when it differs from the previously calculated value by mere 0.001.

Slope stability analysis

Regardless of the different assumptions in the different methods

(Taylor, 1948; Janbu, 1954; Bishop, 1955; Lowe and Karafiath, 1960; Bishop and Morgenstern, 1960; Morgenstern, 1963; Spencer, 1967) available for the analysis of stability of a slope, give values of the safety factor that differ by no more than 5%. Even though it does not satisfy all conditions of global equilibrium; Bishop (1955) simplified method also gives very similar results. Partly because of the good results and partly because of its simplicity, the slice method of limit equilibrium analysis proposed by Bishop (1955) has been used widely for predicting slope stability under both drained and untrained loading conditions. Therefore the present study on analysis of slope has been carried out using Bishop's simplified method (1955).

Choice of critical circle: As per the Fellenius (1927, 1933) method the trial of location of centre was started and then an area could be identified where the possible centre of the critical circle might be located. A number of probable locations of centre were considered in the form of a matrix to identify the critical circle. Different radii were chosen against the pre-defined matrix of locations of centres of the slip circles. The minimum factor of safety has been taken as the critical factor of safety and the corresponding circle has been taken as critical circle.

Horizontal shear stability analysis

In case of the stability analysis of earthen dams the seepage of water is an important factor and the same has to be considered in a proper manner. A horizontal shear may be developed due to seepage and the failure may occur on the downstream side of the embankment. On the other hand, the sudden draw down as in case of the existing embankment at Sundarban a horizontal shear force may be developed on the upstream end of the embankment. The approximate analysis of the stability against the horizontal shear force developed due to seepage and sudden draw down has been carried out as suggested by Creager, et al, (1956).

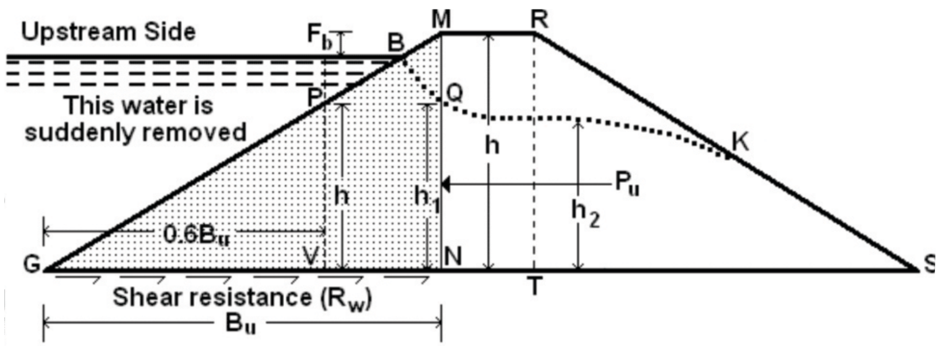

Figure 3: Development of Horizontal Shear at U/s due to Sudden Draw Down

Upstream slope of the embankment during sudden drawdown: The mechanism of failure on upstream side of the embankment due to sudden draw down has been explained in Figure 3. It is based on the simple principle that a horizontal shear force (P_u) is exerted by the saturated soil. The resistance to this force $(R)_u$ is provided by the shear resistance developed at the base of the soil mass, contained within the up steam triangular shoulder.

Considering a unit length of the embankment, the horizontal force P_u is given by equation 1.

$$P_u = \frac{\gamma_1 h^2}{2} \tan^2(45-/2) + \gamma_w h_1^2/2 \qquad (1)$$

Where $_1$ is the weighted density at the center of triangular shoulder up steam and given by equation 2.

$$\gamma_1 = \frac{\gamma_{sub} h_1 + {}_{dry}(h-h_1)}{h} \qquad (2)$$

Shear resistance $(R)_w$ of the up stem slope portion of the embankment developed at the base is given by equation 3. In other way the R_w may be expressed as the equation 4.

$$R_w = C + W\tan\varphi \qquad (3)$$

Where W =the weight of the up steam triangular shoulder of the embankment and C=the total cohesive force developed at base.

$$R_w = C(B_u*1) + ({}_{sub}*0.5*B_u*h) \qquad (4)$$

Now P_u and R_w are known, the factor safety against sliding can be calculated, using the expression: Factor of safety, $F = R_w/P_u$

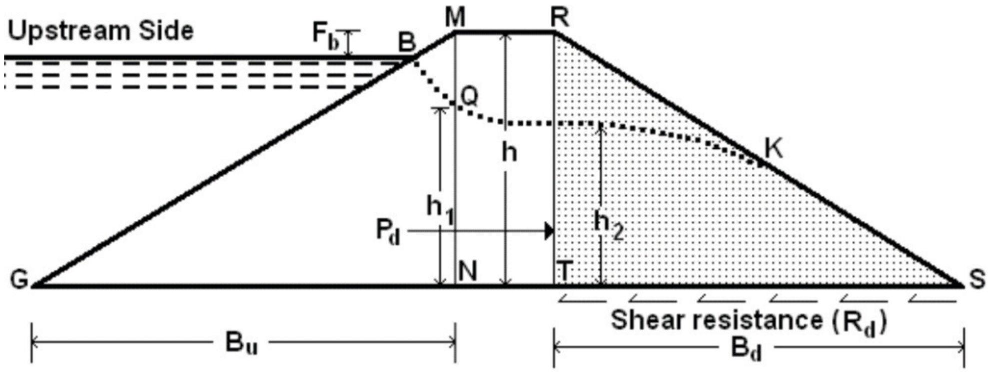

Figure 4: Development of Horizontal Shear at D/s due to Seepage

Downstream slope of the embankment under seepage: The mechanism of failure on downstream side of the embankment due to seepage has been explained in Figure 4. It is based on the simple principle that a horizontal shear force $(P)_d$ is exerted by the saturated soil. The resistance to this force (R_d) is provided by the shear resistance developed at the base of the soil mass, contained within the down steam triangular shoulder.

Consider a unit length of the embankment, the horizontal force p_d is given by equation 5.

$$P_d = \frac{{}_2h^2}{2} * \tan^2(45-/2) + {}_wh_2^2/2 \quad (5)$$

Where ${}_2$is the weighted density at the center of triangular shoulder up steam and given by equation 6.

$${}_2 \frac{{}_{sub}h_2 + {}_{dry}(h-h_2)}{h} \quad (6)$$

Shear resistance $(R)_d$of the up stem slope portion of the embankment developed at the base is given by the following equation 7. In other way the $R_d$may be expressed as the equation 8.

$$R_d = C + W\tan\ \varphi \quad \textbf{(7)}$$

Where, W =the weight of the up steam triangular shoulder of the embankment and C=the total cohesive force developed at base.

$$R_d = CB_d + ({}_{dry}A_1 + {}_{sub}A_2)\tan \quad (8)$$

Now $P_u$and R_w are known, the factor safety against sliding can be calculated, using the expression: Factor of safety, $F = R_d/P_d$

Results And Discussion

The existing embankments at Sundarban are experiencing different hydrodynamics condition spatially and temporally. The prevailing hydrodynamic conditions are (a) coastal hydro-dynamics experiencing wave dynamics, and tidal surge and storm surge, (b) macro tidal effect experiencing the unsteady draw down and tidal surge, (c) meso tidal effect experiencing the unsteady draw down, and (d) effect of meandering of creek, experiencing the river current at the toe or face of the embankments. In the light of the different tidal environment, different geometry of the embankments and average soil condition, the slope stability and the stability against horizontal shear have been considered in the present study. The different tidal conditions have been considered in terms of freeboard or pore water pressure, while the geometry has been considered through height and slope of the embankments.

Slope Stability Analysis

The slope stability analysis has been carried out for total stress and effective stress condition; however, the effect of earthquake has not been considered in the analysis because of the low height (2.0m to 4.0m) of the embankments. The different geometry (height and slope) of the embankments and different pore water pressure has also been considered in the analysis as parametric study.

The results of the slope stability analysis have been enumerated below in Table 2.

The values of Factor of Safety (FoS) has been noted separately (bold and italic) if it become less than 1.5 in case of total stress analysis, while 1.3 in case of effective stress analysis. The noted values are indicating the failure cases in slope stability analysis. Failure occurred in 19 cases at different embankment geometry and pore pressure coefficient.

As revealed from the results of the slope stability analysis (Table 2) that the factor of safety was decreasing gradually in both total stress and effective stress method, as the slope was increasing from 1:1 to 1:2.5 and the factor of safety also decreasing with the increase in pore water pressure (R_u) ranging between 0.3 to 0.5, where the height was kept constant. This follows the general agreement of the slope stability analysis.

Embankment Geometry		Factor of Safety Obtained from Slope Stability Analysis			
Height (m)	**Slope (1:X)**	**Total Stress Method**	**Effective Stress Method**		
			R_u = 0.3	**R_u = 0.4**	**R_u = 0.5**
2.0	1.0	3.92	3.45	3.33	3.20
	1.5	3.29	2.76	2.61	2.53
	2.0	2.99	2.54	2.49	2.44
	2.5	2.40	2.00	1.95	1.90
2.5	1.0	3.05	2.50	2.40	2.35
	1.5	2.35	2.03	1.97	1.91
	2.0	2.05	1.67	1.61	1.55
	2.5	1.78	1.50	1.45	1.38
3.0	1.0	2.37	1.92	1.87	1.82
	1.5	1.93	1.57	1.51	1.46
	2.0	1.67	1.35	1.32	***1.28***
	2.5	1.59	***1.29***	***1.27***	***1.11***
3.5	1.0	1.96	1.61	1.57	1.53
	1.5	1.75	1.42	1.36	1.31
	2.0	1.52	***1.28***	***1.18***	***1.14***
	2.5	***1.37***	***1.15***	***1.10***	***1.01***
4.0	1.0	1.72	1.42	1.34	***1.27***
	1.5	1.58	1.32	***1.21***	***1.13***
	2.0	***1.43***	***1.21***	***1.10***	***1.00***
	2.5	***1.29***	***1.08***	***1.00***	***0.92***

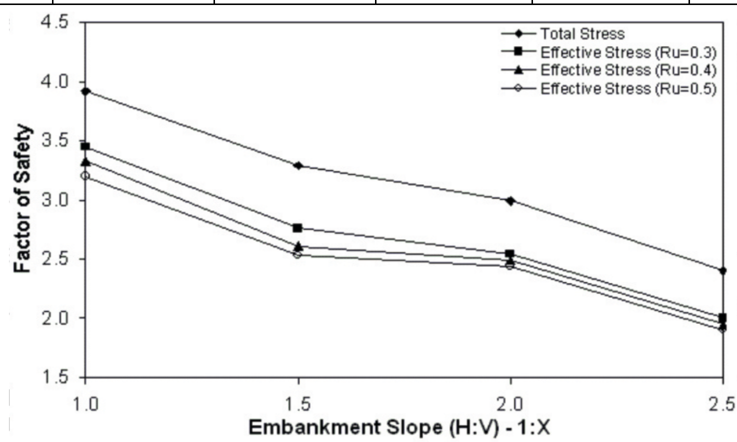

Figure 5: Effect of Geometric and Hydraulic Conditions on Factor of Safety in Slope Stability for Specific Height of Embankment 2.0m

Figure 5 shows that the rate of decrease in factor of safety was low upto the slope 1:2 and then the rate was higher upto 1:2.5, both for total and effective stress method of analysis. The change in factor of safety due to change in pore water pressure was not significant. The failure did not occur for the embankment height of 2.0m. The maximum factor of safety was obtained 3.92 in case of total stress method and minimum was 1.9 in case of effective stress (R_u=0.5) method. However, in case of embankment height 4.0m as shown in Figure 6, the rate of decrease in factor of safety was although almost linear, except very few cases. The change in factor of safety due to change in pore water pressure was significant. The change in factor of safety 0.1 was observed due to change in pore pressure coefficient 0.1. The maximum factor of safety was obtained 1.72 in case of total stress method, while minimum was 0.92 in case of effective stress (R_u=0.5) method. The Figures 5 and 6 represent the two extreme heights for slope stability analysis.

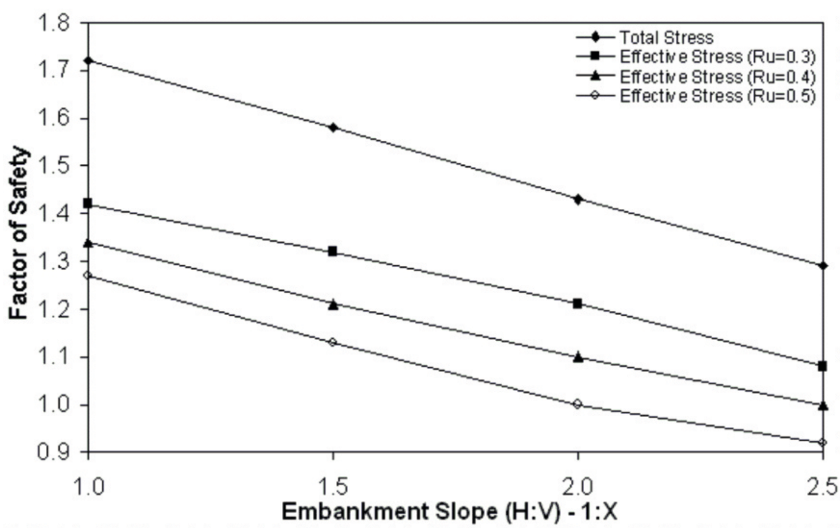

Figure 6: Effect of Geometric and Hydraulic Conditions on Factor of Safety in Slope Stability for Specific Height of Embankment 4.0m

The Figures 7 and 8 indicate that the factor of safety was decreasing almost in parabolic nature both in case of total stress and effective stress method, as the height was increasing from 2.0m to 4.0m, and the factor of safety was also decreasing with the increase in pore water pressure $(R)_u$ ranging between 0.3 to 0.5, where the slope of the embankment kept constant.

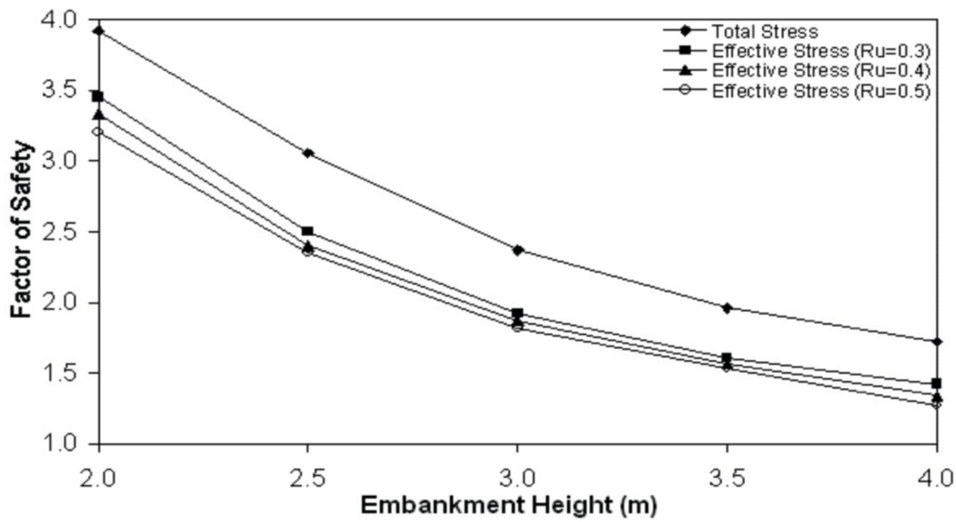

Figure 7: Effect of Geometric and Hydraulic Conditions on Factor of Safety in Slope Stability for Specific Slope of Embankment 1:1

The difference in factor of safety due to increase in pore water pressure was increasing as the slope of the embankment was increasing. The only case of failure occurred in case of the embankment slope 1:1 was at the pore pressure coefficient 0.5 and the height 4.0m (Figure 7); while in case of embankment slope 1:2.5 and the height ranged between 3.0 and 4.0m for effective stress, this included 4.0m height for total stress method also (Figure 8).

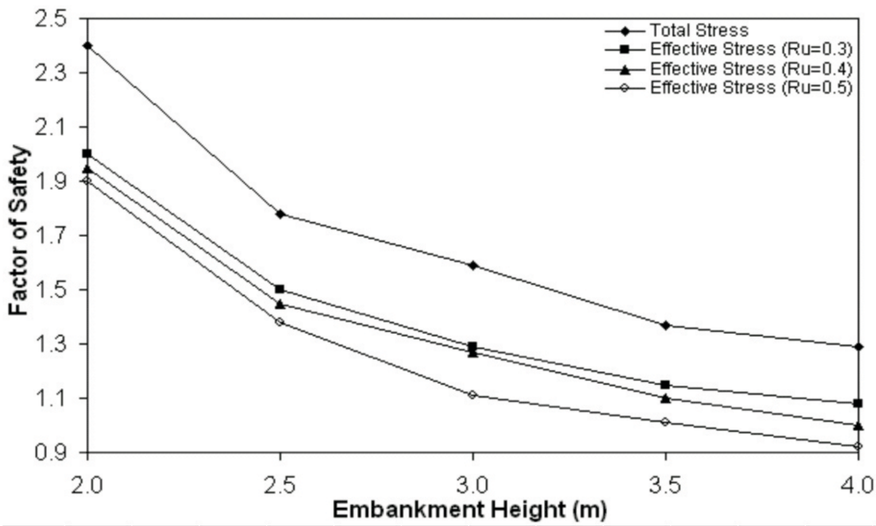

Figure 8: Effect of Geometric and Hydraulic Conditions on Factor of Safety in Slope Stability for Specific Slope of Embankment 1:2.5

The Figures 5 through 8 have been presented herein as typical results of slope stability analysis for extreme geometry of the embankment.

Horizontal shear stability analysis

This analysis has been carried out in consideration with the variation of embankment height and slope considered as in the earlier case of slope failure, but the freeboard was considered as third parameter. The free board shows a strong influence on stability of embankment against horizontal shear, as revealed from the study.Upstream slope of the embankment during sudden drawdown*: Due to sudden draw down of a horizontal shear force developed at the base of the embankment, which is normally responsible for failure at upstream end. The variation height of the embankment as considered in the present study was 2.0m to 4.0m and slope 1:1 to 1:2.5. Free board, the important influencing factor for stability against horizontal shear force has been considered to be varied 0.0m to 1.0m, at an increment of 0.25m. The results of this analysis have been enumerated below in Table 3.*

Freeboard (m)	Height (m)	Factor of Safety Obtained from Horizontal Shear Analysis due to Drawdown (Upstream)			
		Slope			
		1:1	1:1.5	1:2	1:2.5
0.00	2.0	***1.18***	***0.78***	***0.60***	***0.44***
	2.5	***0.97***	***0.64***	***0.48***	***0.37***
	3.0	***0.83***	***0.54***	***0.40***	***0.31***
	3.5	***0.72***	***0.45***	***0.35***	***0.27***
	4.0	***0.64***	***0.42***	***0.32***	***0.25***
0.25	2.0	***1.45***	***0.93***	***0.75***	***0.62***
	2.5	***1.13***	***0.78***	***0.60***	***0.48***
	3.0	***0.93***	***0.67***	***0.49***	***0.37***
	3.5	***0.78***	***0.58***	***0.41***	***0.30***
	4.0	***0.71***	***0.50***	***0.37***	***0.27***
0.50	2.0	1.55	***1.12***	***0.90***	***0.74***
	2.5	***1.24***	***0.94***	***0.72***	***0.58***
	3.0	***1.01***	***0.78***	***0.58***	***0.45***
	3.5	***0.85***	***0.65***	***0.47***	***0.36***
	4.0	***0.78***	***0.56***	***0.41***	***0.33***
0.75	2.0	1.89	***1.25***	***1.02***	***0.76***
	2.5	***1.47***	***1.00***	***0.83***	***0.62***
	3.0	***1.18***	***0.83***	***0.67***	***0.49***
	3.5	***0.96***	***0.71***	***0.55***	***0.41***
	4.0	***0.87***	***0.62***	***0.46***	***0.37***
1.00	2.0	2.26	***1.43***	***1.26***	***1.03***
	2.5	1.69	***1.16***	***0.97***	***0.76***
	3.0	***1.34***	***0.97***	***0.77***	***0.57***
	3.5	***1.07***	***0.79***	***0.63***	***0.45***
	4.0	***0.96***	***0.69***	***0.50***	***0.41***

Table 3: Critical Factor of Safety at Upstream Face of Embankments against Horizontal Shear Stability due to Drawdown for Different Geometrical and Hydraulic Conditions

The factor of safety varies in hyperbolic manner with the height of the embankment, when the slope of the embankment and free board kept as constant; however, this pattern of change in factor of safety could be seen in almost all the cases of different slopes (Table 3). It has also been revealed from the table 3 that the factor of safety was increased with the increase in free board. Occurrence of failure of embankment noted in all the cases of geometry of embankment and hydraulic condition considered in this analysis, except four cases. Hence, the horizontal shear force due to sudden drawdown may be identified as one of the major reason of distressed condition of Sundarban embankments.

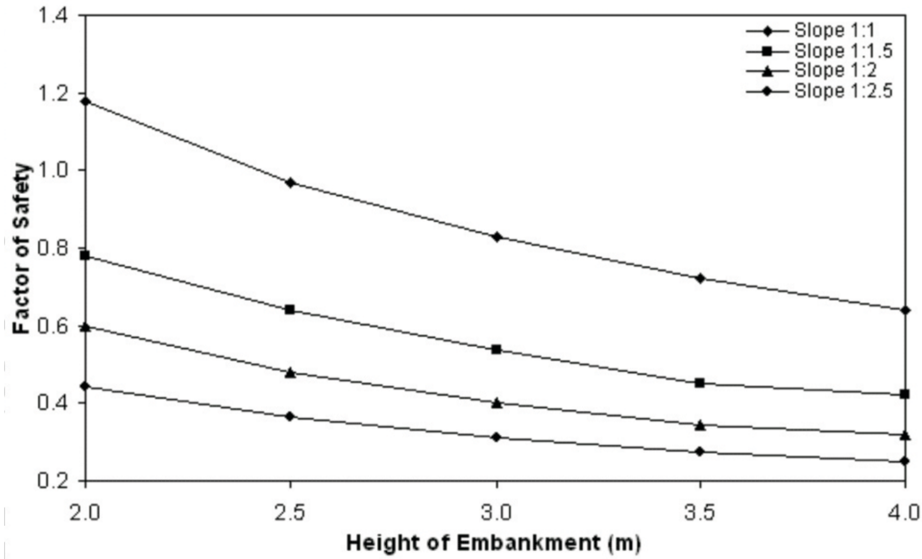

Table 3: Critical Factor of Safety at Upstream Face of Embankments against Horizontal Shear Stability due to Drawdown for Different Geometrical and Hydraulic Conditions

For visual sensation of change in Factor of Safety, Figure 9 has been presented as a typical figure considering the varying geometry of the embankment and free board 0.00m. In case of the varying height and 1:1 slope of the embankment for free board 0.00m the factor of safety was slightly higher, than the other cases such as slope 1:1.5 to 1:2.5 of same free board, though all the cases was obtained as failure cases for free board 0.00m.

Downstream slope of the embankment under seepage: The stability analysis of the downstream end of earthen embankments considering the horizontal force at base developed due to seepage has been carried, which includes the different height with different slopes as geometrical parameters of embankments and different freeboard as hydraulic parameters.

The results of the downstream stability analysis due to horizontal force developed due to seepage has been presented in Table 4, which shows that the major occurrence critical condition for slope 1:2 and 1:2.5.

Freeboard (m)	Height (m)	Factor of Safety Obtained from Horizontal Shear Analysis due to Seepage (Downstream)			
		Slope			
		1:1	1:1.5	1:2	1:2.5
0.00	2.0	2.17	1.65	***1.22***	***0.76***
	2.5	1.83	***1.34***	***0.98***	***0.68***
	3.0	1.51	***1.10***	***0.82***	***0.59***
	3.5	***1.30***	***0.98***	***0.73***	***0.51***
	4.0	***1.14***	***0.90***	***0.65***	***0.46***
0.25	2.0	2.55	1.87	***1.43***	***0.87***
	2.5	1.92	1.51	***1.09***	***0.76***
	3.0	1.55	***1.21***	***0.90***	***0.68***
	3.5	***1.34***	***1.06***	***0.82***	***0.61***
	4.0	***1.22***	***0.98***	***0.82***	***0.60***
0.50	2.0	3.00	2.20	1.70	***1.11***
	2.5	2.22	1.72	***1.26***	***0.94***
	3.0	1.76	***1.37***	***1.03***	***0.79***
	3.5	1.50	***1.19***	***0.88***	***0.68***
	4.0	***1.39***	***1.16***	***0.87***	***0.62***
0.75	2.0	3.00	2.35	***1.84***	***0.95***
	2.5	2.49	1.86	***1.40***	***0.79***
	3.0	2.03	1.53	***1.10***	***0.70***
	3.5	1.69	***1.31***	***0.96***	***0.66***
	4.0	1.50	***1.20***	***0.87***	***0.66***
1.00	2.0	4.00	2.60	2.00	***1.11***
	2.5	2.88	2.00	1.52	***0.93***
	3.0	2.20	1.62	***1.22***	***0.82***
	3.5	1.79	***1.44***	***1.06***	***0.71***
	4.0	1.60	***1.31***	***1.03***	***0.65***

Table 4: Critical Factor of Safety at Downstream Face of Embankments against Horizontal Shear Stability Analysis due to Seepage for Different Geometrical and Hydraulic Conditions

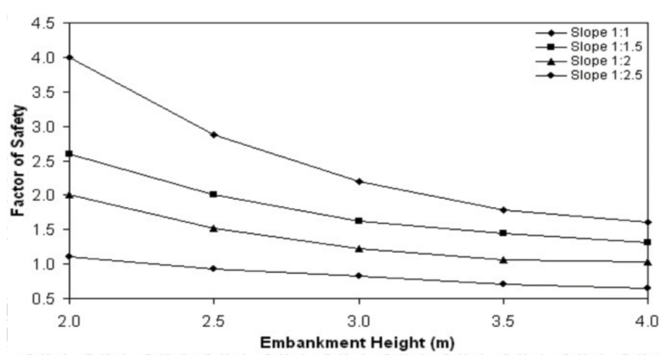

Figure 10: Effect of Geometry of Embankment on Factor of Safety in Horizontal Shear Stability for Specific Freeboard 1.00m and Seepage

The pattern of the curves as presented in Figure 10 may be noted as hyperbolic to linear for different slopes of the embankment, when height has been kept as variable in X axis. The Figure 10 has been presented herein as a typical case for a constant freeboard 1.00m, the other values of freeboard have also been considered for analysis but the pattern of the curve was almost similar. It may also be noted that the pattern of the curves were obtain almost similar to the upstream analysis, as presented in Figure 9.

The study reveled that the existing embankments of Sundarban is probably not becoming distressed due to slope failure, but may be due drawdown effect of the tidal water in the creeks.

Conclusion

The shear strength value of the subsoil and embankment soil of the study area was low. The failure of the embankments in the Sundarban deltaic system may have different causes, but in the present study it was found that the embankments were mostly safe in slope stability, except few cases especially when reservoir is full (i.e. high tide). But the same was found unsafe in the base shear (up steam and down steam) in most of the cases. In case of horizontal shear stability analysis the factor of safety became much less value than the allowable factor of safety. However, more analysis is required to identify the possible causes of failure of existing embankments of the study area. The following conclusions may be drawn from the present study:

1) The existing embankments are safe against slope stability except few cases. Factor of safety is on the higher side, however the same may be in critical state for higher heights and steeper slope such as 3.0m to 4.0m height and slope 1:2 and 1:2.5
2) In cease of the stability analysis due to horizontal shear force, the upstream embankment shows the critical condition in almost all the cases except few, indicates the probable causes of failure of existing embankments at the study area.
3) In case of downstream stability analysis due to horizontal force developed due to seepage the critical condition occurred for slope 1:2 and 1:2.5 and the other slopes were found to be safe for heights upto 4.0m, and even 0.0m freeboard.

Acknowledgement

The author acknowledges the Department of Civil Engineering, Jadavpur University for providing the

fund to carryout the subsoil investigation programme.

References

1. Bishop, A.W., (1955), "The use of the Slip Circle in the Stability Analysis of Slopes", *Geotechnique*, Vol. 5; pp. 7-17.
2. Bishop, A.W., and Morgenstern, N.R., (1960), "Stability Coefficients for Earth Slopes", *Geotechnique*, Vol. 10; pp.129-150.
3. Creager, Justin, and Hinds, (1956), "Engineering for Dams", Vol. III, John Wiley & Sons, New York.
4. Chakraborty, P., (1991),"Morphostratigraphy of coastal quaternaries of West Bengal and Subarnarekha Delta, Orissa", *Indian Journal of Earth Science*, Vol. 18, No.3-4, pp 219-225.
5. Desai, C.S., and Sherman, W.C, (1971), "Unconfined Transient seepage in sloping banks ", *Journal of the Soil Mechanics and Foundation Division,* ASCE
6. Desai, C.S., (1972), "Seepage Analysis of Earth Dams under Drawdown", *Journal of the Soil Mechanics and Foundation Division*, ASCE.
7. Dvinhoff, A.H and Harr, M.E (1971), "Phreatic surface location after drawdown", *Journal of the Soil Mechanics and Foundation Division* ASCE, Vol. 97, no SM 1, pp.47-58.
8. Das, B.K., and Bhandari, G., (2005), "A Preliminary Study on Identification of Probable Causes of Failure of Existing Earthen Embankments around Sundarban", Unpublished Master Degree Thesis, Submitted at Jadavpur University.
9. Fellenius, W., (1927), "Erdstatische Berechnungen mit Reibung und Kohaesion", Ernst, Berlin.
10. Fellenius, W., (1933), "Calculation of stability of earth dam, *Trans. 2 nd Congress on Large Dam*, Vol. 4, p. 445.
11. Janbu, N., (1954), "Application of Composite Slip Surfaces for Stability Analysis", European Conference on 'Stability of Earth Slopes', Stockholm, Discussion 3.
12. Lowe, J., and Karafiath, L., (1960), "Stability of Earth Dams upon Draw Down", Proceedings of *First Panamerican Conference on Soil Mechanics and Foundation Engineering*, Mexico City, Vol. 2, pp.537-552.
13. Morgenstern, N.R., (1963), "Stability Charts for Earth Slopes during Rapid Draw down', *Geotechnique*, Vol. 13, No. 2; pp.121-132.
14. Spencer, E., (1967), "A Method of Analysis for Stability of Embankments using Parallel Inter Slice Forces", *Geotechnique*, Vol. 17, pp. 11-26.
15. Taylor, D.W., (1948), "Fundamentals of Soil Mechanics, Wiley, New York, pp 700.

STATIC AND DYNAMIC BEHAVIORS OF GEOCELL REINFORCED SOFT CLAY

Ashim Kanti Dey
Professor, Department of Civil Engineering, NIT Silchar, Silchar- 788010,
E-mail ashim_kanti@yahoo.co.in
Prasenjit Debnath
M.Tech research scholar, Department of Civil Engineering, NIT Silchar, Silchar- 788010,
E-mail prasen458@gmail.com

Abstract

Soft clay is normally avoided during construction due to its low bearing capacity and high susceptibility of consolidation. The safe bearing capacity of soft clay is considerably increased with insertion of geocells at a suitable depth from the foundation level. Although it is known that geocell reinforced soft clay behaves differently in confined and unconfined conditions, but a detailed study is not reported yet. Moreover, the behavior of geocell reinforced soft clay under dynamic loading is also not properly studied. Extent of increase in bearing capacity of soft clay due to insertion of geocells is also not known. Present research is intended to carry out a series of static and cyclic triaxial tests in confined and unconfined conditions and to understand the effect of geocells on modification of strength parameters and dynamic properties of soft clay. It is observed that under unconfined conditions, the geocells will compress resulting in increase in strain, whereas, under confined condition, the geocells will stiffen the soil resulting in increase in stress. It is also observed that maximum improvement in axial stress is achieved when the geocells are placed at a depth of one fourth of the loading diameter. However, position of geocells does not have a significant effect on stress strain curve in unconfined condition. The stress strain curve of geocell reinforced clay shows an early rise in stress. It is observed that the shear modulus increases and the damping ratio decreases due to insertion of geocells in soft clay.

1. Introduction

During the last three decades geosynthetics are being extensively used to improve the properties of poor soil, like to increase the drainage property, to reduce the compressibility, to improve the shear strength, etc. In order to increase the bearing capacity of soft clay, use of geocells is also being extensively used [Bush et al., 1990], [Cowland and Wong, 1993], [Hendricker et al., 1998], [Dash, et.al., 2001], [Leshchinsky and Ling, 2013], [Fakher and Jones, 1996], [Madhavi and Vidya, 2007], [Selig and McKee, 1961], and so on. Dash et al. (2003) reported that provision of geocell reinforcement improves the load carrying capacity of foundation soil. Normally a geocell is a three-dimensional, honey-comb like structure made of geosynthetics interconnected by joints. Geogrids are normally used to make the cage and geotextiles or geomembranes are put inside the cage for retaining the filling material like sand, gravel or boulder. The geocells may be triangular, square, rectangular or hexagonal in plan depending upon the nature of utility. Geocells have been found to be useful for base reinforcement of embankments and subgrade soil, reinforcement below shallow foundations and steep slopes and in other applications where the soil should withstand high tensile stresses. Flexural rigidity of the geocells plays an important role in increasing the strength of soil against bending. In the present study, effects of geocells in modifying the shear strength of soft clay under static and dynamic loading have been undertaken. A series of triaxial compression tests have been carried out on 75 mm diameter clayey soil samples reinforced with four interconnected geocells placed at different depths from the top of the sample. Cyclic triaxial tests have also been conducted on the samples to find out the improvement on dynamic properties of soft clay, due to insertion of geocells. A considerable improvement in the static and dynamic properties has been observed.

2. Materials Used For Testing

Locally available silty clayey soil which has 60% fines finer than 75 micron was used for the present study. Fig. 1 shows the particle size distribution of this soil. The liquid limit, plastic limit and specific gravity of the soil were found to be 52%, 27%

and 2.54 respectively. As per Unified Soil Classification System (USCS), the soil is classified as inorganic clay with high compressibility (CH). The undrained in-situ shear strength of the soil obtained through vane shear test was found to be 6.5 kPa at a density of 20.73 kN/m^3 and water content 40.2%. All the laboratory tests were performed on remolded samples prepared through four steps. The steps were to dry the clay lumps, grind the lumps into fine powder, add requisite quantity of water and finally consolidate the sample into the desired density. Water content was tried to keep around 40%. The size of each soil sample was kept as 75 mm diameter x 150 mm height. Four interconnected geocells, each of size 20 x 20 x 20 mm were prepared with geo-grid. A layer of geomembrane (locally available plastic sheet, 0.09 mm thick) was put inside the geogrid. Coarse sand was poured into each cell. Fig. 2 shows the picture of the geocells used in the present study. The geocells were placed at different depths inside the soil sample as shown in Figs. 3 and 4. Table 1 shows the properties of the georid. Gradation curve of the coarse sand which was used to fill the geocells is also shown in Fig. 1. The sand has a uniformity coefficient (C) of 2.28, coefficient of curvature (C) of 1.11 and specific gravity of 2.6. The soil is classified as poorly graded sand with nomenclature SP according to the USCS soil classification system. For all the tests the sand was compacted to a density of around 16 kN/m^3 (i.e. 70% relative density) for filling the geocells. Direct shear tests of this density show that the angle of shearing resistance is 39^0.

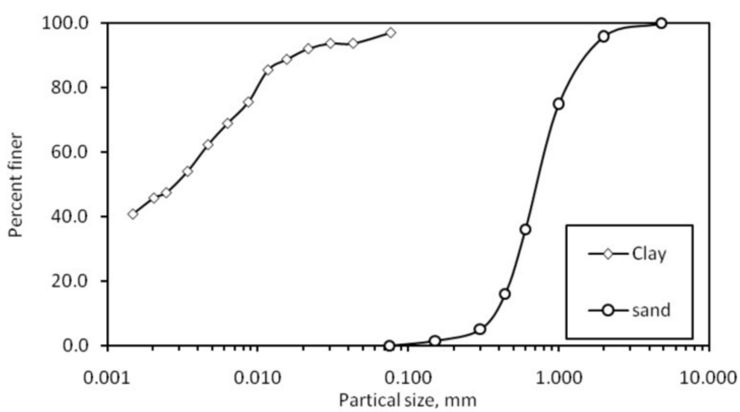

Figure 1 Particle size distribution of the clay and sand used in the study

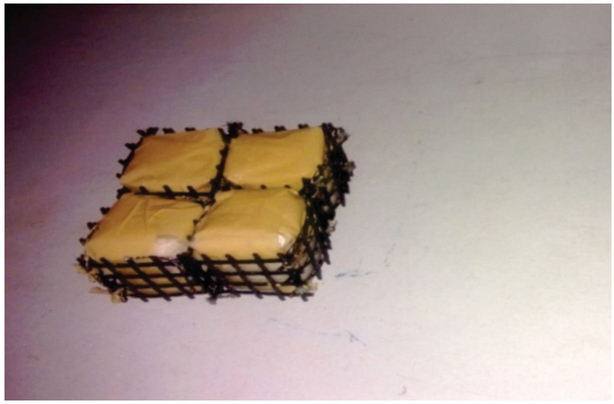

Figure 2 Four interconnected geocells used in the present study

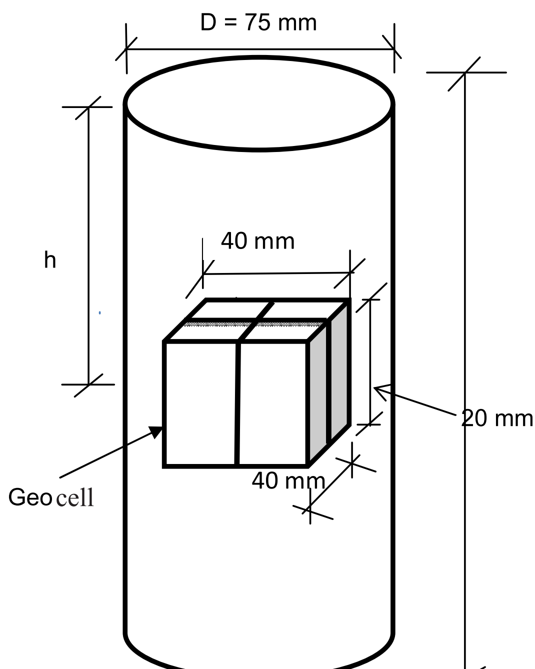

Figure 3 Placement of geocell inside the soil sample

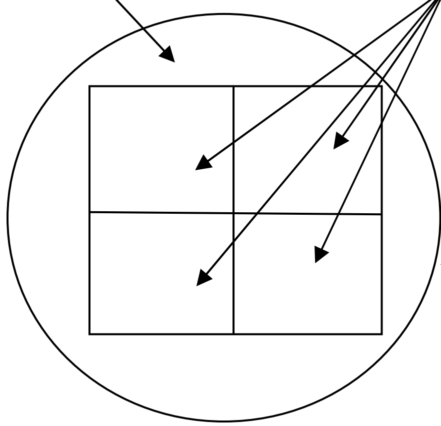

Figure 4 Cross section through soil sample with geocells

Parameter	Value
Polymer	Polypropylene
Aperture size (MD*XMD)	6mm*5mm
Peak tensile strength (MD*XMD)	4.8 kN/m*5.5kN/m
Yield point strain (MD*XMD)	23%*20%
Aperture opening shape	Rectangle

MD: machine direction, XMD: cross-machine direction.

Fig. 5 shows the stress - strain curve of the four geocells containing geomembrane encapsulated sand as shown in figure 2. It is observed that the geocells filled with sand get compressed under a compressive load, follow an elastic path upto around 30% strain, pass through plastic state upto 62% strain and then fail by rupturing.

The result suggests the possible use of present form of geocells as an elastic material upto 20% strain.

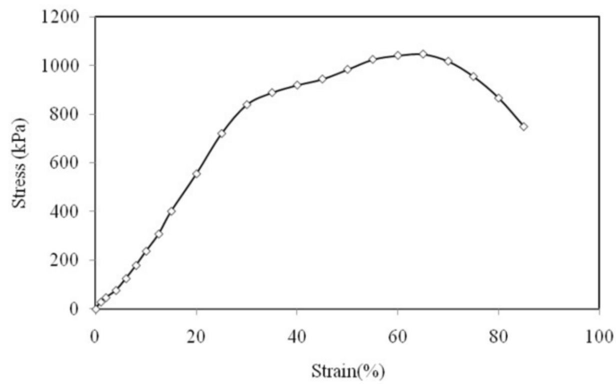

Figure 5 Stress- strain behavior of geocell

3. Test Programme

It was decided to conduct both static and cyclic triaxial tests on 75 mm diameter soil samples. In one set of tests a confining pressure of 100 kPa was applied, whereas in other set of tests no confining pressure was applied for obtaining the unconfined compressive strength. In order to obtain the degradation of strength due to cyclic loading, 30 cycles were given to each sample under displacement control mode, with displacement amplitude ± 1 mm and frequency of loading 1 Hz. Soon after the cyclic loading, the sample was sheared under unconsolidated undrained condition to find the degraded shear strength. The position of geocell was varied for different tests. The total test programme is shown in Fig. 6.

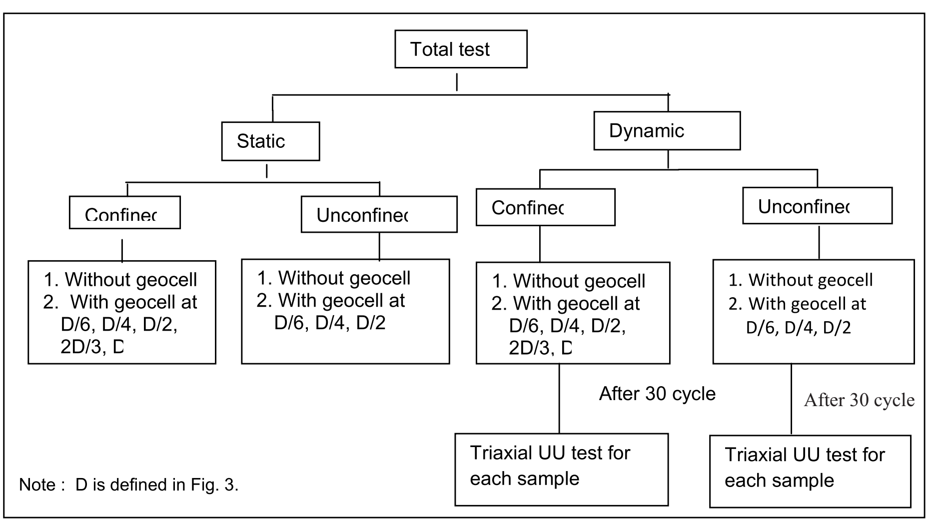

Fig. 6 Test programme.

4. Results And Discussion

4.1. Static Triaxial Test

Typical stress-strain curves from the static triaxial UU tests with and without confining pressures are shown in Figs. 7 (a) and (b) respectively. The position of geocell from the top of the sample is also shown in the figure. For a comparison purpose, the stress strain curve for the normal soil sample without any geocell is superimposed on the figure. It can be seen that for geocell reinforced soil no failure stress is achieved. However, in this study, a stress corresponding to 20% strain is considered to be the failure stress. In addition to the increase in the strength of soil, there was a corresponding increase in the stiffness of the soil, which is indicated by steeper stress strain curves as in Figs. 7(a) and (b). Rajagopal et. al. 1999 also reported an increase in stiffness of geocell reinforced sand samples. Their results also showed that failure does not occur even at 20% strain. As obvious, the maximum failure stress for geocell reinforced clay is more than that for unreinforced clay. This increase in strength is due to enhanced confinement effect [Bathurst and Karpurapu, 1993]. In the present study maximum increase in deviator stress is observed when the geocell is placed at a depth of D/4 from the top of the sample. This may be compared with the results obtained by Dash et. al 2001 who obtained the optimum depth of geocell as 0.1B for sandy soil.

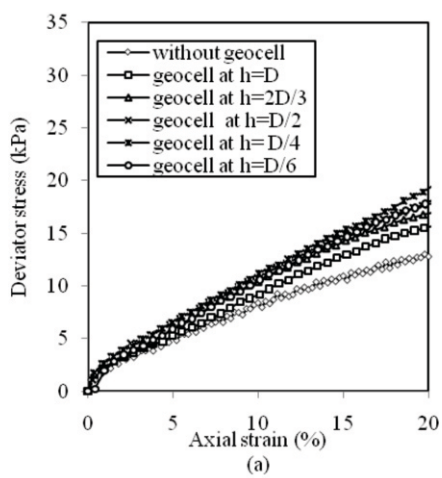

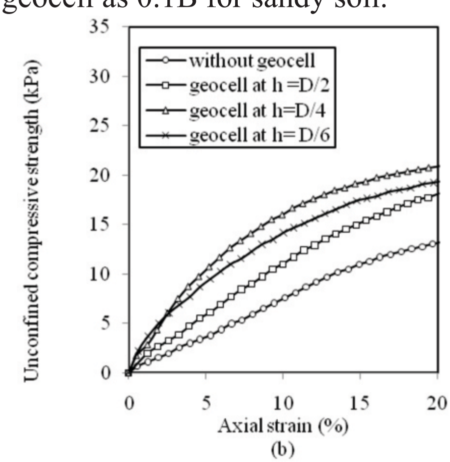

Figure 7 (a) Deviator stress-strain for soil samples with and without geocell with confining pressure = 100 kPa.
(b) Unconfined compressive strength against strain for soil samples with and without geocell

A term, known as Improvement Factor is defined as a ratio of deviator stress of geocell reinforced soil to that of unreinforced soil corresponding to 20% strain. The variation of improvement factor for the confined and unconfined tests is shown in Figs. 8 (a) and (b) respectively. It is observed that the improvement factor increases with strain for confined tests implying that a properly confined geocell will take a higher load. An unconfined soil on the other hand takes a high load at low strain upto 2 to 3%. At large strain the improvement factor for unconfined soil is around 1.5 irrespective of position of geocells. This indicates that a geocell reinforced clayey soil takes a higher load either in confined or unconfined condition.

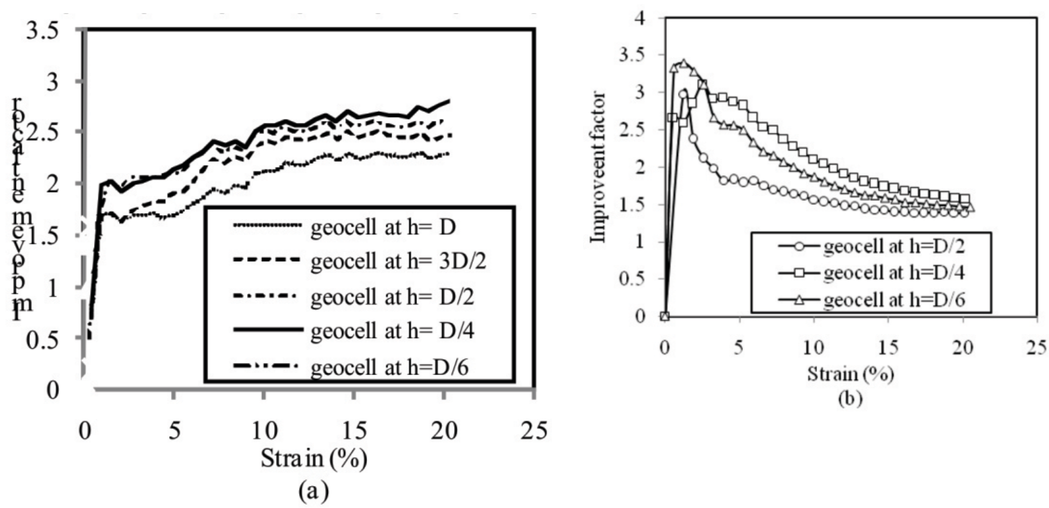

Figure 8 Improvement factor against strain: (a) with confining pressure 100 kPa. (b) Without confining pressure

4.2 Cyclic Triaxial Test

Cyclic triaxial tests were conducted on geocell reinforced soil samples with and without confining pressures. 30 load cycles at 1 Hz frequency were applied under displacement control mode with amplitude ± 1 mm. Typical stress strain loops of clayey soil are shown in Figs. 9 and 10 with and without geocells respectively. Seed and Idriss, 1971 gave a concept of equivalent number of uniform load cycles to represent an earthquake;

using their concept, 30 number of uniform load cycles indicate an earthquake magnitude of 8. Static triaxial UU tests were conducted on each sample after application of 30 cycles to observe the variation of residual strength due to installation of geocell reinforced soft clay. Variation of deviator stress against strain under static tests is shown in Fig. 11 (a) with confining pressure and variation of unconfined compressive strength against strain in Fig. 11 (b). It is also observed that after cyclic loading, the failure deviator stress is more for geocell reinforced soil than that for unreinforced clay. Maximum increase in deviator stress is observed when the geocell is placed at a depth of D/4 from the top of the sample.

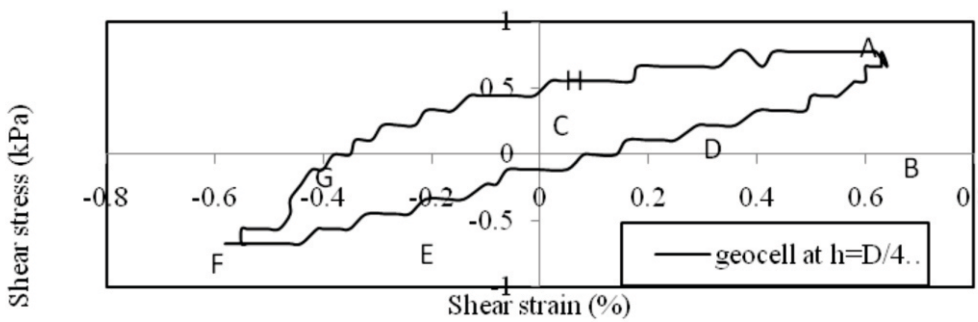

Figure 9 Shear stress - shear strain loop of geocell reinforced clay with confining pressure = 100 kPa.

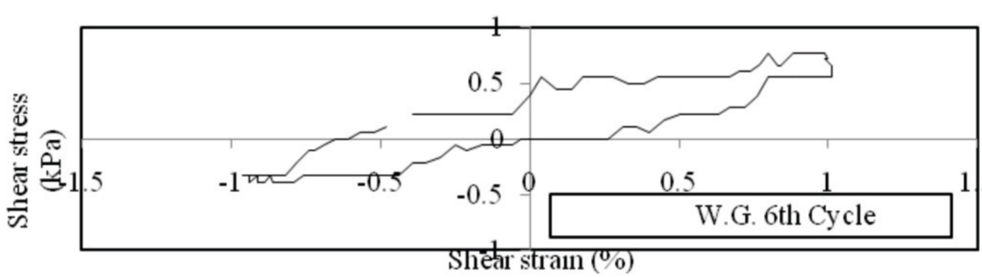

Figure 10 Shear stress - shear strain loop of unreinforced clay with confining pressure = 100 kPa.

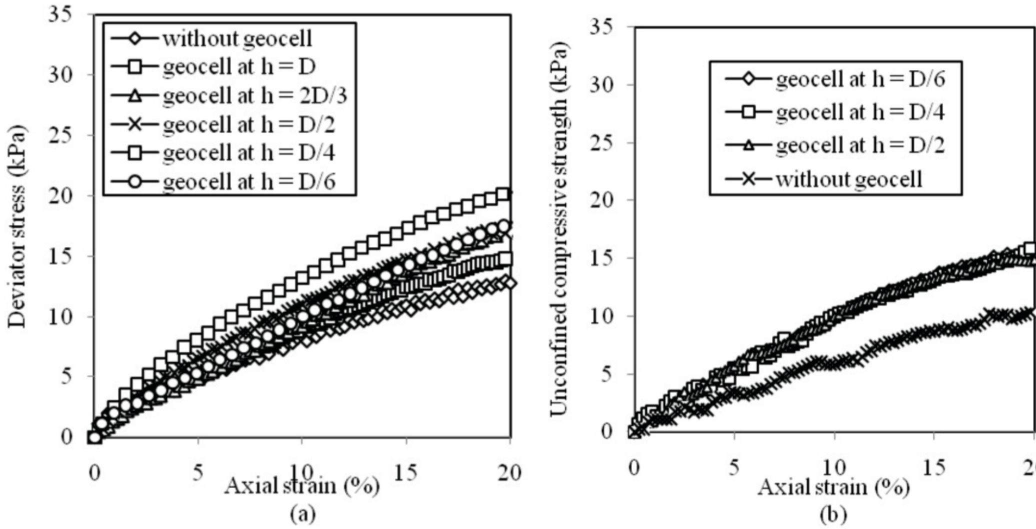

Figure 11 (a) Deviator stress against strain after 30 cycles of loading with confining pressure 100 kPa (b) Unconfined compressive strength against Strain after 30 cycles of loading.

A comparison of failure deviatoric stress before and after dynamic loading is also made to find the degree of degradation, which is defined as reduction in deviator stress due to cyclic loading to the deviator stress without cyclic loading. It is observed that cyclic loading has degraded the strength of geocell reinforced soil. Table 2 shows the % degradation of axial stress for confined and unconfined tests. It is observed that degradation of normal soft clay is around 4% whereas for geocell reinforced soft clay the degradation is around 2-3% under confined condition except for the case where geocell was placed just below the loading plunger (h=D/6), degradation for this position is around 5%. For unconfined condition, geocell reinforced soft clay has a high degradation value, around 15 -20%. Thus the geocells are not effective in reduction of degradation of soft clayey soil under cyclic loading. In unconfined condition the degradation due to installation of geocells are even more than the normal soil. This indicates a limitation of applications of geocells under unconfined condition and placing just below the foundation.

Table 2 Percentage degradation of deviator stress and unconfined compressive strength due to cyclic loading corresponding to 20% strain.

Position of geocell,h (cm)	Confined			Unconfined		
	Deviator Stress (kPa) at 20% strain	Deviator Stress (kPa) at 20% strain after 30 loading cycles	% of degradation	Unconfined compressive strength (kPa) at 20% strain	Unconfined compressive strength (kPa) at 20% strain after 30 loading cycles	% of degradation
h=D/6=1.25	18.64	17.66	5.26	19.13	15.7	17.93
h=D/4=1.875	20.5	20.1	1.95	21.58	16.19	24.98
h=D/2=3.75	17.66	17.17	2.77	17.67	14.72	16.70
h=2D/3=5.00	16.87	16.68	1.13			
h=D=7.50	15.67	15.2	3.00			
Without geocell	12.75	12.26	3.84	12.75	10.79	15.37

Variations of failure deviatoric stress against location of geocell for all the above triaxial tests are shown in Fig 12 From the figure it is observed that the failure deviatoric stress increases with increase in placement depth of geocell from the top; attains a maximum value with geocells at D/4 and then decreases with increase in placement depth. It is thus concluded that the maximum deviatoric stress is obtained when the geocells are placed at D/4 even after a certain number of loading cycles

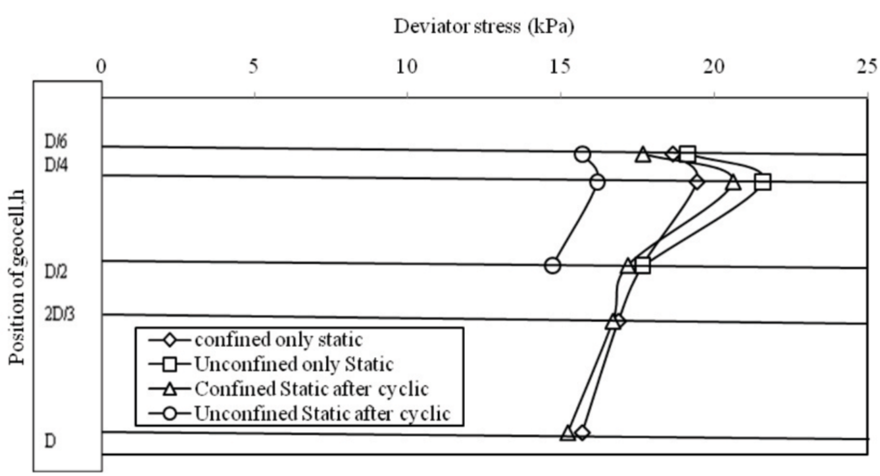

Figure 12 Variation of deviator Stress with position of geocell.

4.3 **Dynamic Test Results And Discussions**

When a soil is subjected to a cyclic loading, the stress strain curve forms a loop called a hysteresis loop, the area of the loop shows the energy dissipated during a cycle. The loop can be described by two parameters, namely, inclination to the strain axis and width of the loop. The inclination of the hysteresis loop depends upon the stiffness of the soil, and is defined by a term called secant shear modulus, G_{sec}, which is tangent of the angle intercepted by a line joining two vertices of the loop with the strain axis.

Figs. 13 (a) and (b) show the changes of secant shear modulus with the variation of no. of cycles for confined and unconfined cyclic triaxial compression tests. From the graphs it may be clearly seen that when the geocell is at D/4 from the top, the value of secant shear modulus is the highest of all the values. Variation of secant shear modulus against number of cycles for unreinforced soil is also shown in the figures. It can be seen that the secant shear modulus of unreinforced soil is always the lowest for both confined and unconfined conditions.

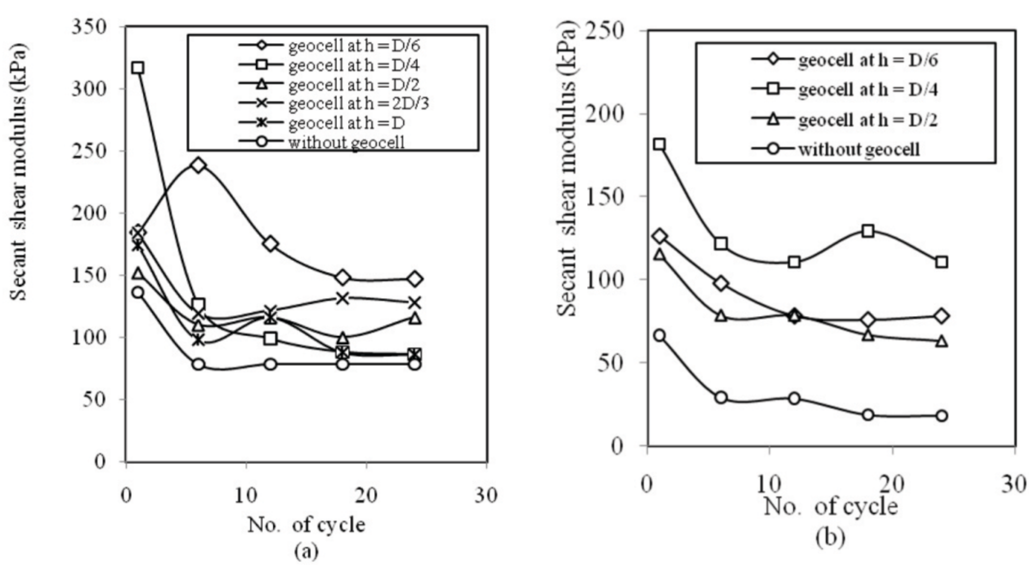

Fig. 13 Secant shear modulus against number of cycles: (a) with confining pressure 100 kPa (b) without confiningpressure.

Considering the changes in the value of shear modulus due to placement of geocells, a term named as 'Modification factor' is defined as the ratio of a geocell reinforced soil property to the corresponding unreinforced soil property. Variation of modification factor of secant shear modulus with number of loading cycles for different positions of geocell is shown in Figs. 14 (a) and (b) with and without confining pressures. It is observed that under confined condition, the modification factor does not follow a definite trend for different positions of geocells, whereas under unconfined condition the modification factor shows an increasing trend with number of cycles. This indicates that stiffness of geocell reinforced soft clay increases with increase in number of loading cycles – the maximum increase occurs when the geocell is placed at D/4. The main reason for this increase is due to the fact that under cyclic loading the soft soil compresses under unconfined condition. Although some trend is observed for the modification factor when the geocells are placed at D/4, however, no definite conclusion can be drawn with these few tests.

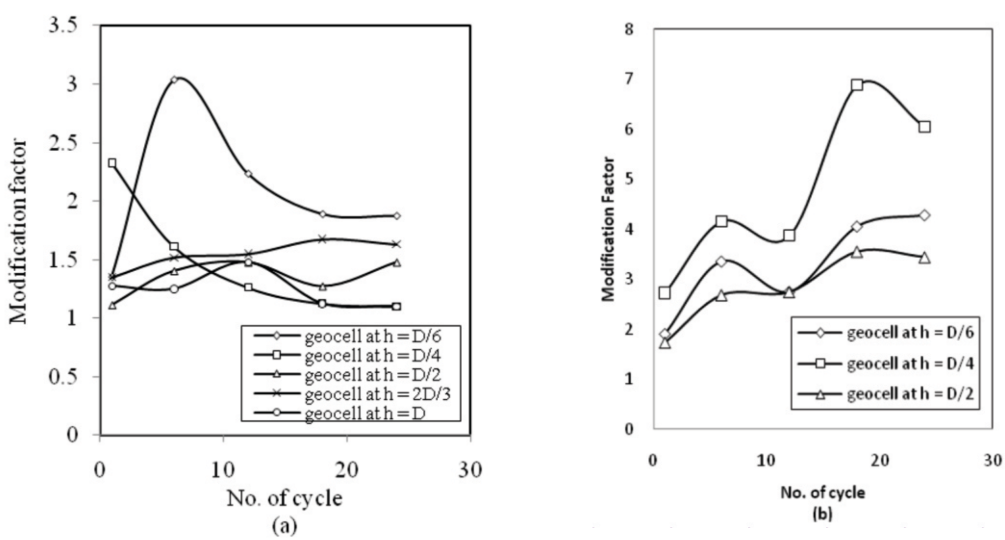

Figure 14 Modification factor for secant shear modulus against number of cycles: (a) with confining pressure 100 kPa (b) without confining pressure.

Normally, the damping ratio is defined as the ratio of damping coefficient (c) to the critical damping coefficient (c_c), however, it can also be defined as the ratio of the area of the loop (A_{loop}) AEFGHA to the area of the triangle ($A_{triangle}$) ABC through the following equation:

$$\text{Damping ratio } (\zeta) = \frac{A_{loop}}{4*\pi*A_{triangle}} \qquad (1)$$

The definition is further explained in Fig. 9. Variation of damping ratio with number of loading cycles is shown in Figs. 15 (a) and (b) for confined and unconfined tests. From the figures it is clearly seen that under a confining pressure of 100 kPa the damping ratio of unreinforced clay lies between 5 to 6.5% up to 25 numbers of loading cycles; whereas, with geocell reinforcement, the damping ratio reduces to 2 to 4% for the same number of loading cycles. However, a high damping ratio is observed for unconfined and unreinforced soil sample. Fig. 15 (b) shows that the damping ratio of unreinforced soft clay increases to 20% after 25 numbers of loading cycles under unconfined conditions. This implies that although soft clay has a property of amplifying the vibration amplitude, but with increase in loading cycles, the damping property of soft clay increases. This property of soft clay can be utilized in reducing the vibration amplitude by adopting soft clay dampers below the foundation [Singh and Dey, 2013].

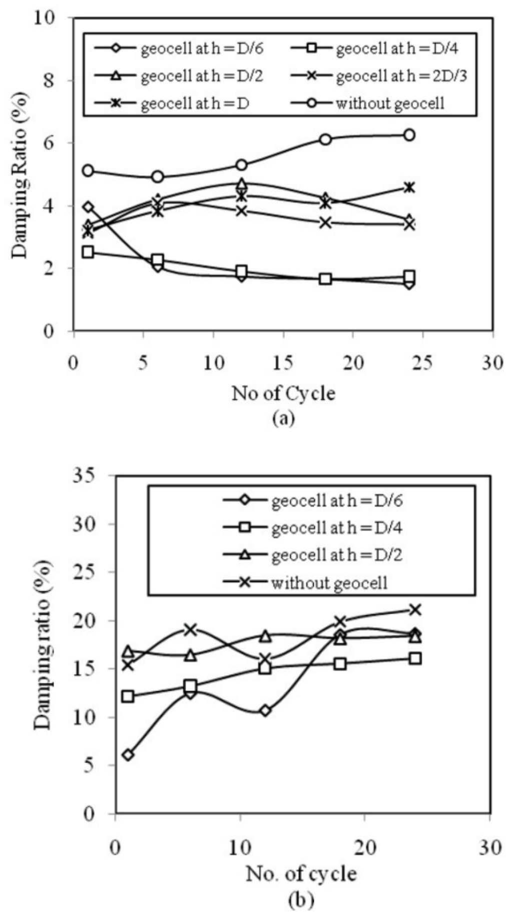

Fig.15 Damping ratio against number of cycle: (a) with confining pressure 100 kPa (b) without confining pressure.

In order to obtain the effect of geocells, modification factor of damping ratio is also calculated. From Figs. 16 (a) and (b) it is noted that with increase in number of cycles, geocell reinforcement reduces the modification factor under confined condition, but increases the modification factor under unconfined condition. Decrease in modification factor with number of cycles indicates that geocell reinforcement decreases the damping ratio with number of loading cycles. For unconfined condition the modification factor for damping ratio is around 0.8 after 25 numbers of loading cycles.

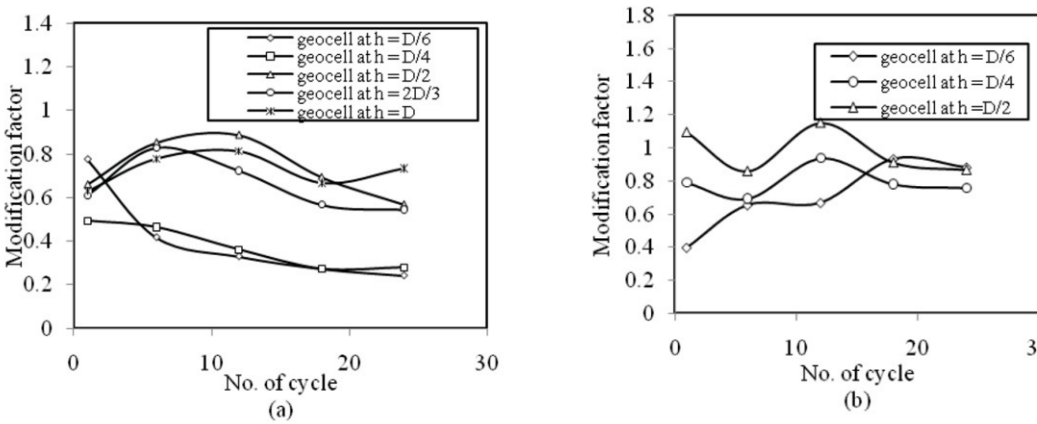

Figure 16 Modification factor for damping ratio against number of cycles: (a) with confining pressure 100 kPa (b) without confining pressure.

5. Summary And Conclusions

This paper has investigated the influence of geocell confinement on the strength and dynamic behaviours of soft clay. The deviatoric strength parameters were determined from the triaxial compression tests. The dynamic behaviours like damping ratio and secant shear modulus were determined from cyclic triaxial tests. Effect of number of loading cycles and positions of geocell on degradation of deviatoric stress has been studied. The water content of the soft clay was tried to be maintained at 40%, near to the liquid limit of the soil. The following conclusions are drawn from the results of this investigation.

1. The induced apparent excessive strength depends on the

position of the geocells from the top of the sample. It is observed that when the geocells are placed at one fourth of the diameter /width of the loading area, maximum benefit in strength is achieved.

2. Geocells reinforced soil does not show any failure stress under unconfined condition.

3. Position of geocells plays an important role on modification of properties of soft clay. Position of geocells under unconfined condition does not have any effect on gain in strength after a number of loading cycles.

4. There is a degradation of strength of soil after some loading cycles, however, the degradation is marginally less once geocells are inserted into the soil provided the geocells are not provided very close to the footing.

5. Lesser damping ratio and higher secant shear modulus are obtained if the soil is reinforced with geocells.

6. The secant shear modulus shows a maximum increase in its value under confined condition when geocells are placed at one-fourth of the loading diameter.

7. The improvement factor of deviatoric stress does not depend on the location of the geocells for unconfined conditions.

8. Under a confining pressure of 100 kPa the damping ratio of unreinforced clay lies between 5 to 6.5% upto 25 number of loading cycles; whereas, with geocell reinforcement, the damping ratio reduces to 2 to 4%. However, a high damping ratio of 20% is observed for unconfined and unreinforced soil samples.

References

[1] Bathurst, R.J., Karpurapu, R. 1993. Large scale triaxial tests on geocell reinforced granular soils. Geotechnical Testing Journal 16 (3), 296-303.

[2] Bush, D.I., Jenner, C.G., Bassett, R.H., 1990. The design and construction of geocell foundation mattress supporting embankments over soft ground. Geotextiles and Geomembranes 9, 83-98.

[3] Cowland, J.W., Wong, S.C.K., 1993. Performance of a road embankment on soft clay supported on a geocell mattress foundation.

Geotextiles and Geomembranes 12, 687-705.

[4] Dash, S.K., Krishnaswamy, N.R., Rajagopal, K., 2001. Bearing capacity of strip footings supported ongeocell-reinforced sand. Geotextiles and Geomembranes 19, 235–256.

[5] Dash, S.K., Rajagopal, K., Krishnaswamy, N.R., 2001b. Strip footing on geocell reinforced sand beds with additional planar reinforcement. Geotextiles and Geomembranes 19, 529–538.

[6] Dash, S.K., Sireesh, S., Sitharam, T.G., 2003. Model studies on circular footing supported on geocell reinforced sand underlain by soft clay. Geotext. Geomembr. 21 (4), 197-219.

[7] Fakher, A., Jones, C.J.F.P., 1996. Discussion of bearing capacity of rectangular footings on geogrid reinforced sand, by Yetimoglu, T., Wu, J.T.H., Saglamer, A.J. Geotech. Eng. ASCE 122 (4), 326e327.

[8] Hendricker, A.T., Fredianelli, K.H., Kavazanjiam, Jr., E., McKelvey III, J.A., 1998. Reinforcement requirement sat a hazardous waste site. In: Proc. of 6th Internat. Conf. On Geosynthetics, Atlanta, USA, Vol. 1, pp. 465-468.

[9] Leshchinsky, B., Ling, H., 2013. Effects of geocell confinement on strength and deformation behaviour of gravel. J. Geotech. Geoenviron. Eng., ASCE 139 (2), 340-352.

[10] Madhavi, G.L., Vidya, S.M., 2007. Effects of reinforcement form on the behaviour of geosynthetic reinforced sand. Geotext. Geomembr. 25 (1), 23-32.

[11] Rajagopal, K., Krishanaswamy, N.R., Latha, G.M., 1999. Behaviour of sand confined with single and multiple geocells. Geotextiles and Geomembranes 17, 171–184.

[12] Seed, H.B., Idriss, I.M. 1971. Simplified procedure For evaluating soil liquefaction potential. Soil Mech. Found. Div., ASCE 107 (9), 1249-1274.

[13] Selig, E.T., McKee, K.E., 1961. Static and dynamic behaviour of small footings. J. Soil Mech. Found. Div. ASCE 87 (6), 29e47.

[14] Singha, S. and Dey, A.K. 2014. Dynamic properties of clay dampers. National Seminar on Geotechnique Today - Prediction, Modelling & Construction, IGS, Kolkata chapter, Kolkata, Feb 28-March 1, pp 141-146.

Instructions for Authors

Essentials for Publishing in this Journal

- Submitted articles should not have been previously published or be currently under consideration for publication elsewhere.
- Conference papers may only be submitted if the paper has been completely re-written (taken to mean more than 50%) and the author has cleared any necessary permission with the copyright owner if it has been previously copyrighted.
- All our articles are refereed through a double-blind process.
- All authors must declare they have read and agreed to the content of the submitted article and must sign a declaration correspond to the originality of the article.

Submission Process

All articles for this journal must be submitted using our online submissions system. http://enrichedpub.com/ . Please use the Submit Your Article link in the Author Service area.

Manuscript Guidelines

The instructions to authors about the article preparation for publication in the Manuscripts are submitted online, through the e-Ur (Electronic editing) system, developed by **Enriched Publications Pvt. Ltd**. The article should contain the abstract with keywords, introduction, body, conclusion, references and the summary in English language (without heading and subheading enumeration). The article length should not exceed 16 pages of A4 paper format.

Title

The title should be informative. It is in both Journal's and author's best interest to use terms suitable. For indexing and word search. If there are no such terms in the title, the author is strongly advised to add a subtitle. The title should be given in English as well. The titles precede the abstract and the summary in an appropriate language.

Letterhead Title

The letterhead title is given at a top of each page for easier identification of article copies in an Electronic form in particular. It contains the author's surname and first name initial .article title, journal title and collation (year, volume, and issue, first and last page). The journal and article titles can be given in a shortened form.

Author's Name

Full name(s) of author(s) should be used. It is advisable to give the middle initial. Names are given in their original form.

Contact Details

The postal address or the e-mail address of the author (usually of the first one if there are more Authors) is given in the footnote at the bottom of the first page.

Type of Articles

Classification of articles is a duty of the editorial staff and is of special importance. Referees and the members of the editorial staff, or section editors, can propose a category, but the editor-in-chief has the sole responsibility for their classification. Journal articles are classified as follows:

Scientific articles:

1. Original scientific paper (giving the previously unpublished results of the author's

own research based on management methods).

2. Survey paper (giving an original, detailed and critical view of a research problem or an area to which the author has made a contribution visible through his self-citation);
3. Short or preliminary communication (original management paper of full format but of a smaller extent or of a preliminary character);
4. Scientific critique or forum (discussion on a particular scientific topic, based exclusively on management argumentation) and commentaries.

Exceptionally, in particular areas, a scientific paper in the Journal can be in a form of a monograph or a critical edition of scientific data (historical, archival, lexicographic, bibliographic, data survey, etc.) which were unknown or hardly accessible for scientific research.

Professional articles:

1. Professional paper (contribution offering experience useful for improvement of professional practice but not necessarily based on scientific methods);
2. Informative contribution (editorial, commentary, etc.);
3. Review (of a book, software, case study, scientific event, etc.)

Language

The article should be in English. The grammar and style of the article should be of good quality. The systematized text should be without abbreviations (except standard ones). All measurements must be in SI units. The sequence of formulae is denoted in Arabic numerals in parentheses on the right-hand side.

Abstract and Summary

An abstract is a concise informative presentation of the article content for fast and accurate Evaluation of its relevance. It is both in the Editorial Office's and the author's best interest for an abstract to contain terms often used for indexing and article search. The abstract describes the purpose of the study and the methods, outlines the findings and state the conclusions. A 100- to
250- Word abstract should be placed between the title and the keywords with the body text to follow. Besides an abstract are advised to have a summary in English, at the end of the article, after the Reference list. The summary should be structured and long up to 1/10 of the article length (it is more extensive than the abstract).

Keywords

Keywords are terms or phrases showing adequately the article content for indexing and search purposes. They should be allocated heaving in mind widely accepted international sources (index, dictionary or thesaurus), such as the Web of Science keyword list for science in general. The higher their usage frequency is the better. Up to 10 keywords immediately follow the abstract and the summary, in respective languages.

Acknowledgements

The name and the number of the project or programmed within which the article was realized is given in a separate note at the bottom of the first page together with the name of the institution which financially supported the project or programmed.

Tables and Illustrations

All the captions should be in the original language as well as in English, together with the texts in illustrations if possible. Tables are typed in the same style as the text and are denoted by numerals at the top. Photographs and drawings, placed appropriately in the text, should be clear, precise and suitable for reproduction. Drawings should be created in Word or Corel.

Citation in the Text

Citation in the text must be uniform. When citing references in the text, use the reference number set in square brackets from the Reference list at the end of the article.

Footnotes

Footnotes are given at the bottom of the page with the text they refer to. They can contain less relevant details, additional explanations or used sources (e.g. scientific material, manuals). They cannot replace the cited literature.
The article should be accompanied with a cover letter with the information about the author(s): surname, middle initial, first name, and citizen personal number, rank, title, e-mail address, and affiliation address, home address including municipality, phone number in the office and at home (or a mobile phone number). The cover letter should state the type of the article and tell which illustrations are original and which are not.